Tellus (1998), 50A, 219–241
Printed in UK – all rights reserved

TELLUS
ISSN 0280–6495

The Western Baltic sea ice season in terms of a mass-related severity index 1879–1992

(II). Spectral characteristics and associations with the NAO, QBO, and solar cycle

By PETER LOEWE* and GERHARD KOSLOWSKI†, **Bundesamt für Seeschiffahrt und Hydrographie, Bernhard-Nocht-Straße 78, D-20359 Hamburg, Germany; †Kurt-Schumacher-Straße 95, D-21629 Neu Wulmstorf, Germany*

(Manuscript received 22 July 1996; in final form 17 October 1997)

ABSTRACT

In this sequel paper, the investigation of the ice winter severity in the Western Baltic is continued in the frequency domain. Spectral analysis of the time series of the mass-related ice index ($V_{A\Sigma}$) reveals prominent quasicycles with periods of 2.3, 5.8 and 7.8 years. The same cycles stand out in the variance spectrum of the winter North Atlantic Oscillation (NAO) index. Variations in the quasibiennial Q_2^3 and intermediate I_5^{10} periodicity ranges (indices give the range limits in years) account for 68.2% of the linear correlation (−0.46) between both time series. A maximum entropy subinterval analysis shows that the spectral variance composition of the $V_{A\Sigma}$ series undergoes significant temporal changes. The relative contribution of the Q_2^3 range is down from 52.7% during $1899_{\pm 20}$ to almost half of this value during $1972_{\pm 20}$. The significance of the I_5^{10} and of short periodic oscillations in the S_3^5 range has in turn increased from about 15% each to 36.8 and 30.7%, respectively. Predictions of ice winter severity based on the spectral characteristics of the full record are thus bound to fail. Some predictive skill for severe ice winters, which occurred with an overall frequency of 24.6%, may be realized from an apparent association with the 11-year solar activity cycle. This association has been most pronounced since the 1950s, about the time the 8-year rhythm started dominating variability. 9 out of 10 severe ice winters eventuated in phase with either high (3) or low solar activity (6). Moreover, almost all of the most severe ice winters occurred when the phase of the quasibiennial stratospheric wind oscillation (QBO) at the Equator was east (west) and, at the same time, solar activity was low (high). The peaks in the $V_{A\Sigma}$ spectrum after WWII reflect the dominance of singular 8-year ice events of modulated strength. This quasicyclic recurrence of strong ice winters in conjunction with the apparent statistical Solar Cycle–QBO–Ice Winter Severity relationship may be cautiously used in ice winter forecasting.

1. Introduction

In a companion paper, Koslowski and Loewe (1994), hereafter referred to as KL, described the severity of the Western Baltic sea ice season in terms of a mass-related ice index: the *accumulated areal ice volume* or $V_{A\Sigma}$. By analogy to accumulated degrees of frost, this index was constructed from the mass-related areal ice volume or effective thickness Nh, based on daily observations of ice concentration N and ice thickness h at 6 stations along the Baltic coast of Schleswig-Holstein (cf. KL Fig. 1). In approximating the time integral of Nh over the ice season, $V_{A\Sigma}$ is a well-suited measure of ice winter severity in regions of maritime climate

* Corresponding author. Email: loewe@bsh.d400.de

where temporal discontinuities and even reversals in the seasonal evolution of the ice cover are nothing particular.

A useful classification of ice winter severity in terms of $V_{A\Sigma}$ was due to *weak* $\leqslant 0.36$ m $<$ *moderate* $\leqslant 3$ m $<$ *strong* $\leqslant 10$ m $<$ *very strong* ($\leqslant 26.83$ m in 1942), which corresponds to net ice winter lengths of $w \leqslant 1$ week $< m \leqslant 1$ month $< s \leqslant 2$ months $< vs$ ($\leqslant 3$ months) and seasonal average effective thicknesses (Nh) of $w \leqslant 5$ cm $< m \leqslant 10$ cm $< s \leqslant 15$cm $< vs$ ($\leqslant 30$ cm).

While no significant trend has been detected for the original $V_{A\Sigma}$ series, temporal analysis of the classified dataset revealed that the frequency of both weak and very strong ice winters has increased at the expense of moderate and strong winter types after 1920. It was further shown that winter severity is inversely correlated with the winter North Atlantic Oscillation index, a high (low) NAO index, implying enhanced (attenuated) westerly winds between Iceland and the Azores, being associated with a weak (strong or very strong) sea ice season in the Western Baltic.

As a natural extension of Part I, a complemental spectral analysis of both the $V_{A\Sigma}$ and the NAO index series is presented here (Sections 3, 4). This analysis includes an examination of the spectral composition of the cross-correlation. Peaks in the spectra that turn out statistically significant are corroborated by their occurrence in physically related datasets.

On account of the non-stationarity of the $V_{A\Sigma}$ series, which shows in jumps of variance around 1920 and 1960 (cf. KL Fig. 3 or Fig. 4 here), the spectral variability of both $V_{A\Sigma}$ and the winter NAO index is investigated in Section 5. This analysis together with the rather simple non-sinusoidal structure of $V_{A\Sigma}$ after WWII leads to a mathematical interpretation of the periodicities of the $V_{A\Sigma}$ spectrum as a set of harmonics with a fundamental period of 16 years (Section 6).

In Section 7, some evidence is produced of an association between ice winter severity, the 11-year solar activity cycle and the quasi-biennial oscillation of equatorial stratospheric winds (QBO).

2. Approach: BT versus ME spectral analysis

For the spectral analysis of the severity of ice winters ($V_{A\Sigma}$) and the strength of the zonal circulation (NAO index), the classical Blackman-Tukey technique was used (Blackman and Tukey, 1958; Mitchell et al., 1966). The percent variance spectrum is obtained by taking the real discrete Fourier transformation of the truncated and weighted sample autocorrelation. As the precision of the estimated autocorrelation coefficients decreases with increasing time lag, coefficients above a maximum number of time lags, also called truncation point m (here $= 35$), were ignored and the remainder were weighted using a Tukey-Hanning lag window. This weighting procedure is equivalent to smoothing the truncated (unwindowed) raw spectrum using binomial weights ($\frac{1}{4}$, $\frac{1}{2}$, $\frac{1}{4}$). The main advantage of the BT technique is that the spectral estimates can be statistically tested for significant deviations from a pre-determined theoretical model spectrum (e.g., Gaussian white noise continuum, red noise simple Markov persistence) representing the underlying stochastic processes. The technique's spectral resolution is poor, however. The number of spectral estimates is limited by the number of autocorrelation coefficients or lags *(m)* that are taken into account. What is more, the frequencies for which these estimates are made cannot be freely chosen but are instead determined by m.

Because of the non-stationarity both of $V_{A\Sigma}$ and of the NAO time series, which is seen in the different statistics for different periods of time (KL), a spectral analysis of subseries (of 41 years length) seemed desirable. To this end, the Maximum Entropy (ME) technique was used (e.g., Andersen, 1974) which is particularly suited to short time series because of its excellent spectral resolution. While ME spectral estimation is possible at arbitrary frequencies, standard tests to assess the significance of spectral peaks are not available (Künzel, 1989). Statistical confidence limits thus are not given here.

In ME spectral estimation, the entropy function $\int \ln P(f) \mathrm{d}f$ is maximised under the constraint that the estimated autocorrelation function of the time series is the Fourier transform of the spectral density $P(f)$. The method is the equivalent of fitting an autoregressive process to the data series (Van den Bos, 1971). Even if the underlying stochastic process is of this type, it remains open of what order it is. But a correct identification of the order M of the autoregressive process is crucial if meaningful spectra are to be calculated.

Overestimating M results in a spuriously peaky spectrum while underestimating it results in too flat a spectrum. For the calculation of the spectra presented here, M was assessed by evaluating Aikaike's FPE criterion (e.g., Jones, 1976). For the complete $V_{A\Sigma}$ series, $M=16$. The optimal order or prediction error filter length for the full NAO series as identified by the FPE criterion is $M=1$. This value, which indicates simple persistence to be the generating process, is of course too low to give good spectral resolution. Thus $M=25$ was used because the final prediction error (FPE) assumed its first secondary minimum for this filter length. The M values were retained in the subseries analysis.

Before carrying out the ME analysis, the time series were standardised. Each date was divided by the standard deviation after subtracting the mean value. This transformation not only normalizes the variance of the time series, but also the area below the resultant ME spectra (Parseval's Theorem). It must be borne in mind that the ME technique represents a spectral density estimator, a direct comparison with the BT variance spectra is thus not possible. Nevertheless, to allow a comparison, the actual ME density spectra of the complete time series were numerically integrated over the same frequency intervals for which BT spectral estimates were determined. The same procedure applied to the evolutional ME analysis of the subseries. The exact frequencies or periods at which peaks occur in the density spectra were determined using a golden section search algorithm (Press et al., 1988). They are shown by symbols in the figures. In the discussion below of the main cycles, reference is made to these quasi-periods.

3. $V_{A\Sigma}$ spectrum

Fig. 1 shows the relative variance spectra of the $V_{A\Sigma}$ time series as obtained by the BT and ME technique. The thin horizontal lines indicate the white noise spectrum (WNL), constructed on the assumption that variance is evenly distributed across the frequencies, and the accompanying confidence levels (CFL). A comparison between the BT spectrum (shaded) and this model spectrum shows that two periodicity ranges of the interannual time scale clearly stand out from the white noise continuum. Variance is concentrated in significant periods of 2.3 years (CFL 99%), 5.8 years (CFL $\simeq$ 95%) and 7.8 years (CFL $>$ 95%).

The ME spectrum, which is characterized by a larger dynamic range (despite integration over the frequency bins), emphasizes these peaks of the spectral variance distribution. An additional maximum springs up near 20 years. The fact that the 2 bins associated with this peak span a periodicity range of 15.6–20–28 years in addition to its average occurrence at 20.8 years (cf. Section 5) seems to justify a brief note. It has been suggested that climatic variations of this length may be associated with the Hale double sunspot cycle (22.28 years), which also shows in cyclic variations of the solar magnetic field (Schuurmans, 1978; Newell et al., 1989; Ghil and Vautard, 1991). Alternatively, it may be asked whether the approx. 20 years cycles observed here can form part of the interdecadal Arctic climate oscillation hypothesized by Mysak et al. (1990). Whatever the reason, time series from the same area, such as the Central England temperature (1659–1974), show a most prominent maximum in this range in addition to the significant periods mentioned earlier (Folland 1983).

Extensive literature on geophysical time series analysis substantiates the significance of the 2.3, 5.8 and 7.8 years periods. Polli (1946, 1950), for instance, shows that periods of 5.6 years and 8 years occur in a large number of time series of atmospheric pressure, air temperature, precipitation, sea level etc. in all parts of the world. A global distribution is likewise found for the 2.3 years period (Landsberg et al., 1963) which was presumably present throughout the post-Pleistocene period (Landsberg, 1962) and which has often been associated with the quasi-biennial-oscillation (QBO) of equatorial stratospheric winds. While the global occurrence of quasi-cyclic variations is often regarded as an indication of external astronomic causes, oscillations in non-linear dynamic systems can occur without external periodic forcing (Geller, 1989). It is still remarkable that 5.8 and 7.8 years cycles, in particular, were detected for the Earth's orbital and rotational parameters (Loutre et al., 1992).

Below we cite some time series investigations which contain the same significant periods as the $V_{A\Sigma}$ series and which are also physically related to ice conditions in the Western Baltic. The BT spectrum of the number of days with ice occur-

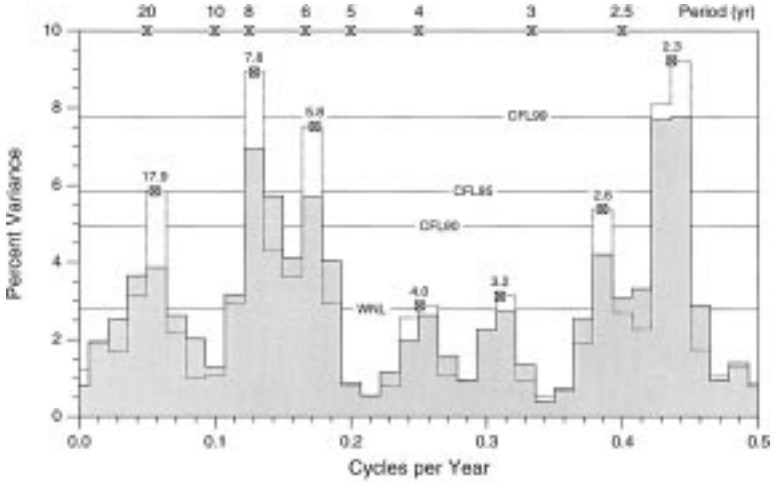

Fig. 1. % variance spectra of *accumulated areal ice volume* ($V_{A\Sigma}$) 1879–1992. The Blackman-Tukey spectrum for maximum lag of 35 years is shown by shaded columns to emphasize the discrete character of this estimator. The level of the white noise continuum (WNL) fitted to this BT spectrum and associated 90, 95, and 99% confidence limits (CFL) are indicated by thin horizontal lines. The dotted column spectrum results from integrating the Burg maximum entropy density spectrum (calculated for 16 prediction error coefficients) over the BT frequency bins. Periods atop checked boxes indentify relative maxima in the ME density spectrum, while sand-glasses just serve as tickmarks for selected periods on the top-axis. The column heights of both the BT- and ME spectrum amount to 100% variance.

rence on the River Elbe (1843–1992) shows prominent peaks at periods of 5.3 years and 7.8 years (Loewe, unpublished); the series of the maximum annual ice extent in the Baltic Sea contains significant cycles of 5.2 years for the period 1808–1893 and of 8 years between 1808–1979 (Alenius and Makkonen, 1981).

Special significance is attached to the time series of the average ice extent in March off the east coast of Newfoundland (Hill and Jones, 1990) which B. T. Hill kindly made available to us (personal communic., 1992). Marko et al. (1986) found a highly positive correlation between the number of icebergs off Newfoundland and ice extent in the Davis Strait. Ice conditions in these regions are inversely correlated with the severity of the sea ice season in the Baltic Sea. Southerly ice advection to the west of Greenland and advection of warm air across the North Atlantic into the Baltic tend to increase or decrease concurrently in response to the strength of the Icelandic low (Rogers and Van Loon, 1979). While, between 1879 and 1991, the maximum ice extent off Newfoundland contained prominent quasi-cycles of 10, 7.8 and 2.3 years, the simultaneous correlation with ice conditions in the Western Baltic in terms of $V_{A\Sigma}$ is of no practical value (-0.15) and barely significant (89%).

4. NAO Spectrum

The connection between the North Atlantic Oscillation as an atmospheric forcing mechanism and ice production along the Baltic coast of Schleswig-Holstein is corroborated by spectral variance analysis of the winter NAO index time series. Fig. 2 shows the BT and ME relative variance spectra for the NAO index between 1879 and 1992. The collective variance content of 25.3% in periodicities >10 years is comparatively high ($V_{A\Sigma}$: 18.0%) and the lag-1 autocorrelation coefficient $\rho(1)=0.16$ is significantly different from 0. A Markovian simple persistence red noise continuum was thus used as a background continuum (Mitchell et al., 1966). According to the χ^2 test, BT cycles of 2.4 and 7.7 years exceed the 90% confidence limits. The ME spectrum additionally shows relatively high amounts of variance at

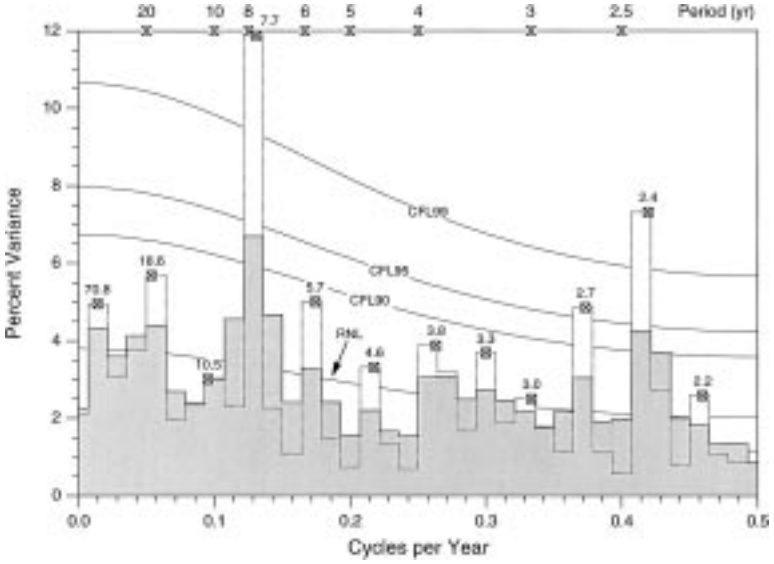

Fig. 2. % variance spectra of the winter NAO index 1879–1992. Superposed on the Blackman-Tukey spectrum (shaded), the red noise continuum determined from the one-year lag autocorrelation coefficient ($\rho(1)=0.16$) is plotted as a thin solid curve (RNL). 90, 95, and 99% confidence limits (CFL) are depicted in the same fashion. For the maximum entropy spectral estimates (dotted columns) 25 prediction error coefficients have been used. Otherwise see caption for Fig. 1.

periods of 2.7, 5.7 and 18.6 years which are even more pronounced in the $V_{A\Sigma}$ spectrum.

What is remarkable is the correspondence between the long periodic cycle of 18.6 years and the length of the lunar nodal cycle (18.6 years). The nodal tide has been found not only to influence variations in sea level, but also appears to affect fluctuations of sea surface temperature, oceanic circulation, variations in atmospheric pressure and general characteristics of atmospheric circulation (Lisitzin, 1974). Specifically, Maximov and Smirnov (1965, 1967) argue that the meridional tidal current due to a global 19 years standing tidal wave gives rise to long-periodic fluctuations in transports of water and heat by the Gulf Stream system, which in turn would induce east-west fluctuations of the Icelandic low. In particular, these authors stress the coincidence of the extremely weak meridional atmospheric pressure gradients between Stykkisholmur (Iceland) and Madeira in January of 1878, 1896, 1916, 1940 and 1955 with the southerly tidal current reaching maximum strength. In a recent paper, Royer (1993) expands on sea surface temperature variations of 0.5–1°C in high latitude oceans as associated with the 18.6 years tide.

To establish the extent to which the autocorrelation of the NAO index data causes inflation of relative variance at lower frequencies and consequent suppression at higher frequencies, the BT relative variance spectrum of the residual series after subtraction of red noise ($R_i = \mathrm{NAO}_i - \rho(1)\,\mathrm{NAO}_{i-1}$) was determined. The residual spectrum deviates significantly (CFL > 90%) from the white noise background continuum, again at periods of 2.4 and 7.7 years.

The cospectrum (Fig. 3) was calculated for $V_{A\Sigma}$ and the residual NAO index so as to avoid overestimation of the cross-correlation coefficients. Fig. 3 shows that the simultaneous inverse correlation of -0.46 between both series is based on cycles of 2.3–2.4, 5.8 and 7.8 years. The cumulative covariance in the quasibiennial Q_2^3 and intermediate I_5^{10} periodicity ranges is 68.2%; the indices give the range limits in years (cf. Table 1). The relative covariance in the long periodicity range (> 10 years) is just 10.4% which is hardly surprising in view of the incoherent course of the low-pass filtered time series (see KL: Fig. 2, 5).

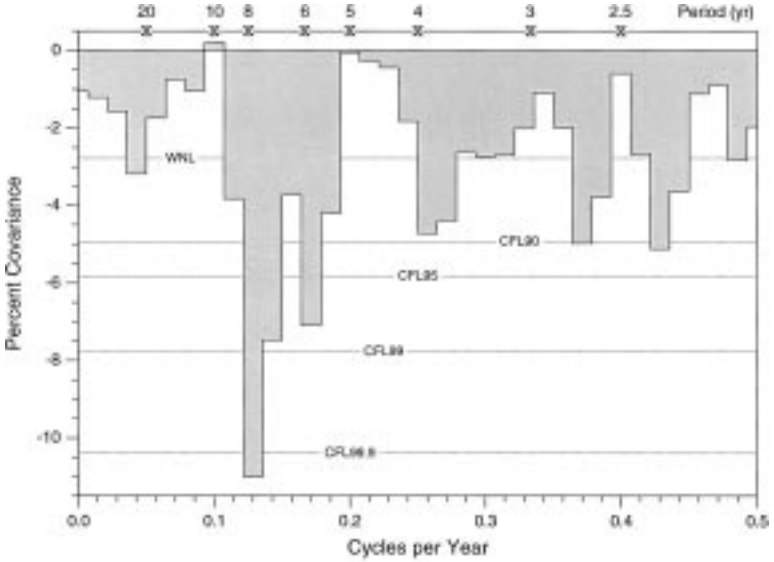

Fig. 3. Co-spectrum of *accumulated areal ice volume* ($V_{A\Sigma}$) and winter NAO index 1879–1992. The white noise null hypothesis (WNL) and associated 90, 95, 99, and 99.9% confidence limits (CFL) are indicated by horizontal dotted lines. Prior to calculating the normalized spectral distribution of the lag-0 cross-correlation coefficient ($\gamma_{xy}(0) = -0.46$) simple Markov persistence ($\rho(1) = 0.16$) was removed from the NAO series (e.g., Dyer, 1970).

Table 1. *Percent band variance of various BT and ME spectra*

Periodicity range ⇝		U_{20}^{∞}	L_{10}^{20}	I_{5}^{10}	S_{3}^{5}	Q_{2}^{3}	$L+U$	$Q+S$	$Q+I$
SLP at PD[1]	ME	10.4	15.6	21.0	26.5	26.5	26.0	53.0	47.5
SLP at A[1]	ME	14.0	10.5	26.2	19.0	30.3	24.5	49.3	56.5
NAO	BT	14.3	11.0	26.3	21.8	26.6	25.3	48.4	52.9
	ME	13.9	11.8	25.6	22.2	26.5	25.7	48.7	52.1
$V_{A\Sigma}$	BT	8.9	9.1	30.8	15.3	35.9	18.0	51.2	66.7
	ME	8.0	9.5	31.3	15.3	35.9	17.5	51.2	67.2
$V_{A\Sigma} \times \text{NAO}^2$	BT	−7.0	−3.4	−37.2	−21.4	−31.0	−10.4	−52.4	−68.2

[1] DJF mean sea level pressure at Ponta Delgada and Akureyri; [2] Co-Spectrum. Periodicity ranges are defined as ultralong (U), long (L), intermediate (I), short (S), and quasi-biennial (Q) with lower and upper indices corresponding to the range limits in years.

What is surprising, however, is the high amount of variance contained in the quasi-biennial periodicity range of the NAO spectrum. This result at least, is at variance with Rogers (1984) who stresses: *the variance in the latter periodicity range [2.1–2.4 years] is notably low in the NAO index*. Our calculations show that the Q_2^3 periodicity range contains 26.6% of the total variance (cf. Table 1); 34.8% is even found for the (white noise) residual spectrum. The significant spectral peak at 2.4 years is the second strongest maximum in the ME spectrum. The inconsistency with Rogers cannot be explained by differences in record length, standardization, or spectral resolution. Spectral estimates of about zero at periods of 2 and 4–5 years (Rogers, 1984, Fig. 3) would appear compatible with the characteristics of a low pass filter which Rogers (1982) applied to a temperature-based NAO index.

The correlation between $V_{A\Sigma}$ and the maximum ice extent off Newfoundland in the interannual and quasi-biennial periodicity ranges implies an enhanced variability of the strength of the Icelandic low in these very ranges (Table 1).

Further evidence of the existence of the quasi-biennial signal in the NAO is found in literature. Brier (1968), for instance, *conclude(s) that the zonal westerlies have a detectable QBO* (quasi-biennial oscillation). Angell et al. (1969) anticipate our result when they write, *The quasi-biennial pressure oscillations in the North Atlantic subpolar Low and subtropical High are almost out of phase, implying a relatively strong quasi-biennial variation in surface zonal wind in North Atlantic temperate latitudes.* To afford the reproduction of our findings, the tabulated winter NAO index is presented in Appendix A.

On the whole, the spectral analysis confirms that anomalies of atmospheric circulation above the North Atlantic Ocean, here expressed in terms of the NAO index, decisively influence ice production along the Baltic coast of Schleswig-Holstein.

5. Spectral variability: evolutional MESA

The non-stationarity of the variance of the $V_{A\Sigma}$ series was pointed out in KL within a subinterval analysis. This phenomenon is caused by abrupt transitions around 1920 and 1960 between relatively stationary levels of variance (KL: Fig. 3). The flat level of variance before 1920 was associated with an enhanced frequency of moderate and strong ice winters (73%) which in the subsequent period of high variance decreased in favour of extreme ice winter types (weak and very strong) to form a relative share of 44%. In view of the fact that later $V_{A\Sigma}$ values are more reliable than those before 1940, the confirmation found in Stellmacher and Tiesel (1989) is convenient. They also note a conspicuously low variability between 1870 and 1925 for the accumulated freezing degree days in Berlin which are indicative of conditions along the Baltic Sea coast.

To suppress the influence on variance of very strong ice winters, a cubic root transformation was performed ($V_{A\Sigma} \mapsto V_{A\Sigma}^{1/3}$) which was suggested by Stidd (1953) in particular for a normalization of Γ-distributed precipitation data. The temporal course of the subinterval variance of the transformed series (Fig. 4) agrees qualitatively with that of the original series (KL: Fig. 3). Interestingly, the maximum ice extent in the whole of the Baltic Sea is characterised by the same sudden changes in variance. Note also the inverse evolution of variance in the ice extent off Newfoundland.

In view of the quasi-periodic variations of the $V_{A\Sigma}$ series as determined in Section 2, questions about the stationarity or persistence of the essential cycles arise. They could be answered by band-pass filtering individual frequency ranges. Another aspect of the stationarity problem is that important cycles may be suppressed in the spectrum of the full series (Fig. 1) because they are (very) active only in certain epochs. The evolutional maximum entropy spectral analysis (EME) provides full information about the dependence

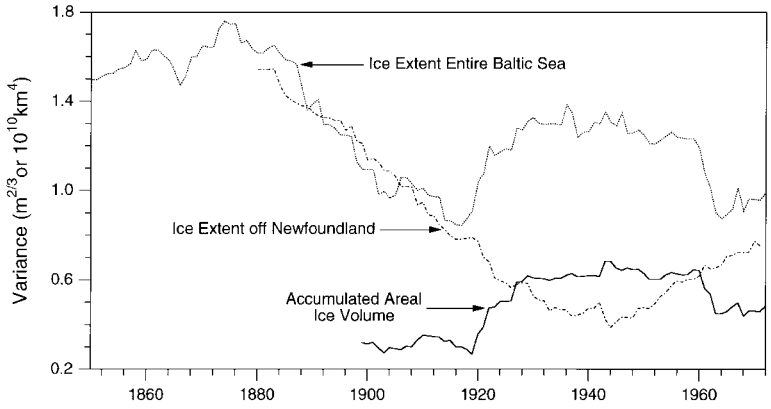

Fig. 4. Temporal evolution of variance for $V_{A\Sigma}^{1/3}$, maximum annual ice extent in the Baltic Sea (Leppäranta and Seinä, 1985), and the ice extent off Newfoundland in March (personal communic. B. T. Hill, Inst. for Marine Dynamics, St. John's, Newfoundland). The variance was calculated for overlapping 41-year intervals and plotted against the central year.

on time of the spectral distribution of variance. A question of particular interest is to what extent sudden changes in variance (see above) are accompanied by discontinuous changes in the spectral distribution of variance.

Fig. 5 shows the EME spectrum of the $V_{A\Sigma}$ series which was partitioned into 74 overlapping 41 years intervals, as was done in KL. Other technical details have been mentioned in Section 1 or are described in the caption. In interpreting Fig. 5, reference is also made to Fig. 6 in which the amount of information was greatly reduced by integration across broader frequency ranges. These frequency or periodicity ranges are identical with those used in Table 1 to summarize the spectra for the full period 1879–1992 as shown in Figs. 1–3. To supplement this Table, the relative and absolute variance contributions of these periodicity ranges are given in Table 2 for 3 time windows which agree roughly with the epochs of relatively stationary variance.

The quasi-periodic character of the different cycles is the most obvious feature in Fig. 5. Even the most stable cycles with the lowest fluctuations in frequency, those in the quasi-biennial frequency range and the 5.8 years cycle, are subject to clear variations in variance content. The strong cycle of 7.8 years only starts in the 1940s, but its strength is such that it stands out as the second strongest maximum in the full spectrum (Fig. 1). The cycles of 3.2 and 4 years have been among the dominating cyclic components of variability only since 1960. They are thus clearly suppressed in the full spectrum.

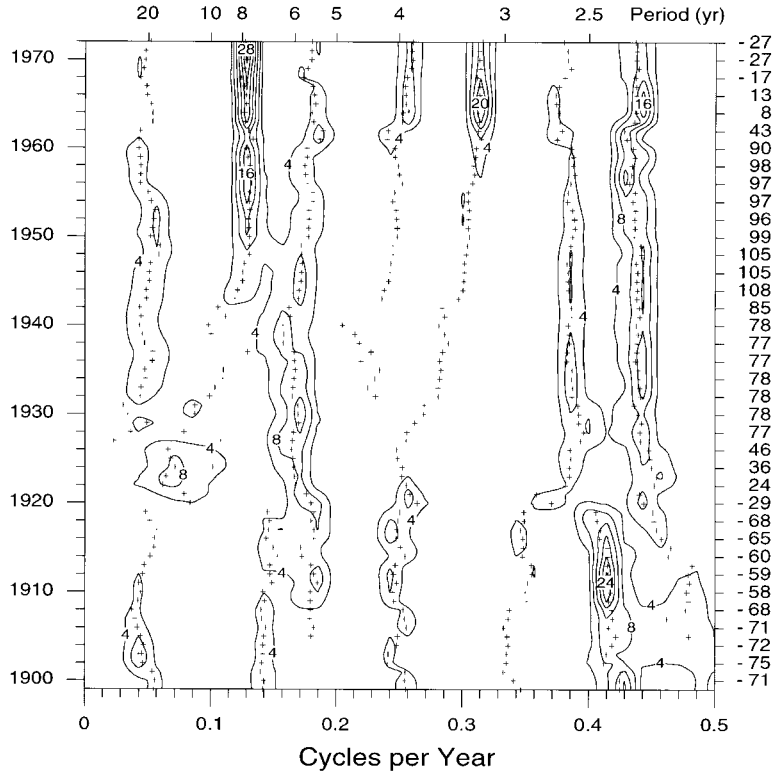

Fig. 5. EME spectrum of $V_{A\Sigma}$ showing the temporal evolution of the spectral variance distribution for overlapping 41-year subintervals of the 114-year record. 74 density spectra were obtained with the Burg ME spectral estimator for 16 prediction error coefficients, integrated over the BT frequency bins of Fig. 1, subjected to binomial smoothing in time-direction, and contoured at intervals of 4% variance. Crosses indicate maxima of the density spectra. As to the significance of the variance maxima see Fig. 1. Labels on the right axis give the relative deviation of total variance of a subseries from that of the full time series.

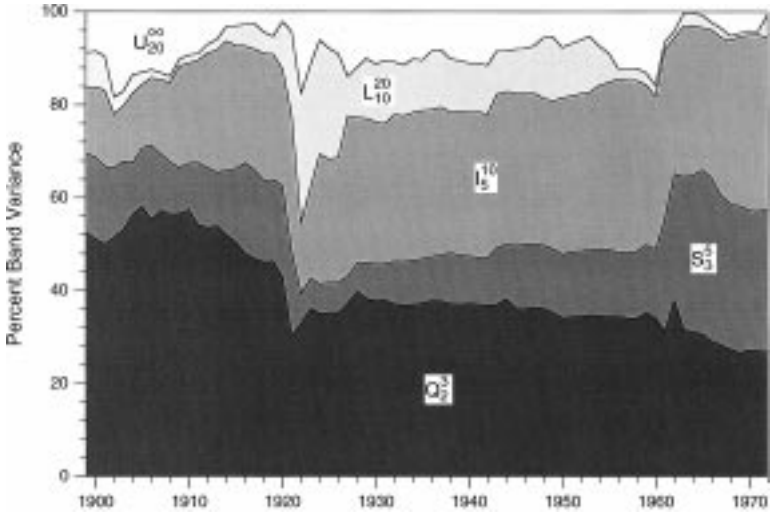

Fig. 6. EME band variance of $V_{A\Sigma}$. The numerical integration of the ME density spectra (underlying Fig. 5) was carried out here for the frequency bands of Table 2. The contributions of relative variance from these bands are stacked against the central year of the proper 41-year time interval.

Table 2. *ME band variance of $V_{A\Sigma}$ for different time windows*[1]

Periodicity range	% Variance			Variance absolute		
	$1899_{\pm 20}$	$1940_{\pm 20}$	$1972_{\pm 20}$	$1899_{\pm 20}$	$1940_{\pm 20}$	$1972_{\pm 20}$
U_{20}^{∞}	8.7	11.1	0.7	0.75	5.71	0.14
L_{10}^{20}	7.7	10.5	4.8	0.66	5.39	1.02
I_5^{10}	14.0	31.0	36.8	1.19	15.99	7.81
S_3^5	16.9	10.1	30.7	1.44	5.22	6.51
Q_2^3	52.7	37.3	27.0	4.50	19.20	5.72
Σ	100.0	100.0	100.0	8.54	51.51	21.20

[1] For a definition of periodicity ranges see Table 1.

The spontaneous change of the whole of the spectral variance distribution around 1920 is especially obvious and is evidently connected with the discontinuity of total variance (Fig. 4). The bifurcation of the principal period of 2.4 years is accompanied by a drop in variance of the Q_2^3 periodicity range from 50 to 30%. The relative variance contribution of the S_3^5 range becomes minimal on the disappearance of the 4 years cycle (6%), while the relative variance contained in the low-frequency range ($L_{10}^{20}+U_{20}^{\infty}$) increases abruptly from 9 to 45% (cf. Fig. 6). The increase to the high level of absolute variance, however, is caused by contributions from all ranges, while since 1930 this level has been held mainly by the Q_2^3 and I_5^{10} ranges (cf. Table 2).

The decrease to the low level of variance since 1960 results from the disappearance of the long-periodic contribution and the halving of absolute variance in the Q_2^3 and I_5^{10} ranges. Table 2 reveals that absolute variability in the Q_2^3, L_{10}^{20} and U_{20}^{∞} periodicity ranges in the last section almost is at the same level as absolute variability in the first section. The sustained strength of cyclic variations of about 8, 4 and 3.2 years qualifies the significance of the quasi-biennial cycles.

The EME spectrum of the NAO index is shown in Fig. 7. Until 1940, the subinterval variance of

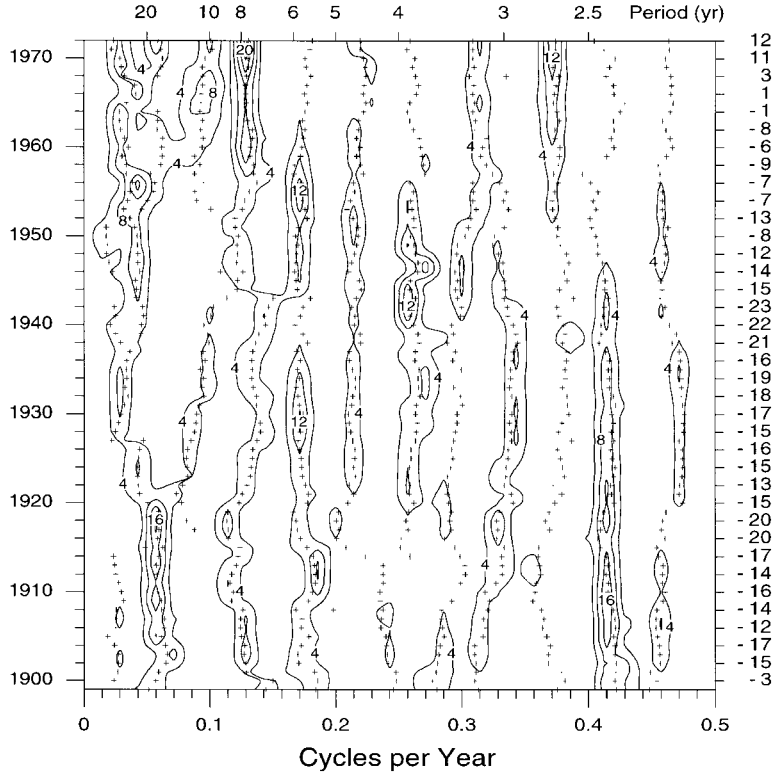

Fig. 7. EME spectrum of the winter NAO index (1879–1992) using 25 prediction error coefficients. See Fig. 2 to get an idea about the significance of the relative variance maxima. Otherwise, see caption of Fig. 5.

the NAO index was about 15% below the variance level of the total series (2.53). Thereafter, a gradual increase is observed, the maximum variance in the last interval ($1972_{\pm 20}$) exceeding this value by 10%. The temporal behaviour of the subinterval variance differs so much from that of the $V_{A\Sigma}$ series that similarities in the time dependence of the spectral distribution cannot be expected.

Around 1920, a bifurcation of the roughly 20 years cycle occurred. The right-hand branch evolved into a cycle of approximately 10 years which has been clearly visible in the EME spectrum of mean sea level pressure at Ponta Delgada since 1930. The increase in absolute variance since 1940 (cf. right scale in Fig. 7) is initiated by increasing variability in the U_{20}^{∞} range and is supported by the revival of the 10 years cycle in the 1950s. The reduction in the 2.4 years cycle in the 1940s is first compensated by greater variance in the S_3^5 range and later by the increasing intensity of the 2.7 years cycle. This latter cycle has been the strongest cyclic variation in the EME spectrum of mean sea level pressure at Ponta Delgada since 1960, but it is of no significance for the EME spectrum for Akureyri where the 8 years cycle has dominated since then.

6. Discussion (harmonics and beats)

There are so many cycles (2.3, 2.6, 3.2, 4, 5.8, 7.8, 17.9 years) that come and go during the 114-years period of the $V_{A\Sigma}$ record that one must wonder which cycles are meaningfully different from the others. Needless to say, the physical reality of none of these cycles can be validated by statistical means. Neither can a decision be made on statistical grounds if they are caused by a single or various physical processes. Since representations in time and frequency domain are equivalent in that they constitute transform pairs of the same

information, spectral peaks are merely indicative of the specific form of a time series.

What can be offered here is the supposition that the observed cycles form a sequence of harmonic oscillations with a fundamental period of 16 years. To illustrate this concept, a harmonic analysis (Panofsky and Brier, 1968) of the $V_{A\Sigma}$ series was carried out for the 48-years record 1945–1992. This time interval is visibly dominated by an 8-years rhythm of strong ice winters (Fig. 5), the first of which occurred in 1947 (cf. KL Fig. 2). While other cycles do exist (Fig. 5), they are not immediately apparent from KL Fig. 2 (or Fig. 10, here). It can be shown, however, that the hidden harmonics (16, 5.3, 4, 3.2, 2.7, 2.3, 2 years) arise from the non-sinusoidal character of the time series.

As documented in Table 3, the variance accounted for by the 3rd, 6th, …, 24th harmonic (H_3 … H_{24}) of the original $V_{A\Sigma}$ series is in good agreement with the results of maximum entropy analysis (Fig. 5). Contributions add up to 84% variance showing that the data are very well approximated by these harmonics. All of them concurrently peak in 1947, 1963, and 1979 when ice winters were most severe. The influence of weak and moderate ice winters ($V_{A\Sigma} \leqslant 3\,m$) can be eliminated from the record by setting $V_{A\Sigma} = 0\,m$ in such years. A re-analysis of the modified series confirms that the periodic characteristics of the time series are determined by strong and very strong ice events (Table 3, column $V_{A\Sigma} > 3\,m$).

Now consider an ideal 8-years rhythm of ice winters of fixed strength, i.e., $V_{A\Sigma}(t_0 + i\Delta t;\ i = 0, 1, \ldots;\ \Delta t = 8$ years$) =$ const. and 0 at other times. Such a sequence of singular signals, though periodic, clearly is a non-sinusoidal function in time. A harmonic representation of this synthetic series can be accomplished but by superposition of the fundamental oscillation of 8 years and its higher harmonics (4, 2.7, 2 years). As the events are of equal strength, each harmonic accounts for the same share of variance (except for the last, contributing half that share). Now, if the ice events recurred after 16 years the variance would be distributed in the same fashion among cycles of 16, 8, 5.3, 4, 3.2, 2.7, 2.3, and 2 years length, which very well correspond with those found by spectral analysis (Fig. 1). It should be realized that these examples bear on the fact that the Fourier transform of a sequence of equidistant δ-functions in time is a sequence of equidistant δ-functions in frequency (Papoulis, 1962).

It can be seen from KL Fig. 2 (or Fig. 10, here) that the winters of 1947, 1963, and 1979 were much more severe than those of 1956, 1970, and 1987. Ignoring all ice winters but those that occurred in $1947 + 8i$, assuming the 1970 event took place in 1971, and bearing in mind the results of the previous paragraph, the distribution of variance for this idealized $V_{A\Sigma}$ series (Table 3, col. $47 + 8i$) is understood as a consequence of the modulation in amplitude of the 8-years rhythm.

Taking into account again all winters of $V_{A\Sigma} > 3\,m$, but exchanging the winters of 1970 and 1971, re-analysis yields column $70 \Leftrightarrow 71$. The differences from the previous case are not utterly insignificant but the main variance contributions still are due to the 8-years cycle and its higher harmonics. On the other hand, a comparison with column $V_{A\Sigma} > 3\,m$ shows that the change in the relative importance of harmonics H_{12} and H_{15}, as well as H_{18} and H_{21}, results from the disturbance of the 8-years cycle in 1970.

A simple approach as to how the amplitude modulation of the 8-years rhythm is realized, is to consider the superposition of either of the harmonic pairs just mentioned. As shown in Appendix B, the superposition of two harmonics of equal amplitude and phase can be written as $\psi = 2A\cos(2\pi\nu^* t)\cos(2\pi\bar{\nu}t)$, where, e.g., $\nu^* = (\nu_{18} - \nu_{21})/2 = (32\ \text{years})^{-1}$ and $\bar{\nu} = (\nu_{18} + \nu_{21})/2 = (2.46\ \text{years})^{-1}$. ψ thus can be interpreted as an almost harmonic oscillation of mean frequency $\bar{\nu}$, whose amplitude $A_{\text{mod}} = 2A(2\pi\nu^* t)$ slowly varies in time at modulation frequency ν^*. ψ is bounded by the envelope $A_{\text{mod}} = \pm[2A^2(1 + \cos(2\pi\nu_{\text{beat}}t)]^{0.5}$ oscillating at twice the modulation frequency $\nu_{\text{beat}} = 2\nu^* = (16\ \text{years})^{-1}$. Note that $\nu_{\text{beat}} = (16\ \text{years})^{-1}$ for any two harmonics H_i and $H_{j=i+3}$. Fig. 8 illustrates the beats arising from superposition of H_{18} and H_{21} of the original $V_{A\Sigma}$ series. The net effect is an amplification of ice events in 1947, 63, and 79 and a reduction in strength around 1955, 71, and 87.

As to the association between $V_{A\Sigma}$ and the winter NAO index, harmonic analysis shows that their 8 years components swing in antiphase (Table 3). As with $V_{A\Sigma}$, the 8-year cycle of the winter NAO index holds the largest share of variance. However, by accounting for merely 52.2%, the set of har-

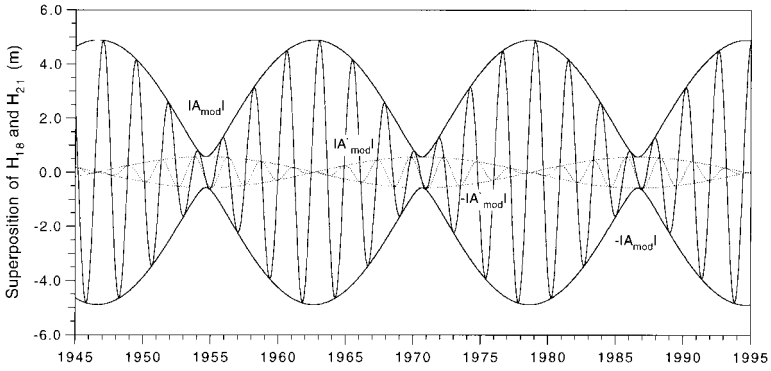

Fig. 8. Superposition of harmonics H_{18} (2.66 years) and H_{21} (2.29 years) of the original $V_{A\Sigma}$ series 1945–1992. The rapidly oscillating solid curve represents $\psi = \psi_{18} + \psi_{21}$ according to eq. (B1) or (B4) of Appendix B and is bounded by $\pm|A_{mod}|$ (cf. eq. (B6)). The dotted oscillations illustrate the secondary beat due to the sine term in eq. (B4).

Table 3. *Harmonic analysis of $V_{A\Sigma}$ (1945–92), synthetic derivatives of $V_{A\Sigma}$, and winter NAO index*

Harm H_k	Period T_k	Phase $t_{k,max}$	% variance of H_k for $V_{A\Sigma}$	$V_{A\Sigma} > 3$[1]	$70 \Leftrightarrow 71$[2]	$47 + 8i$[3]	NAO	Phase $t_{k,min}$
3	16.0	49.2	2.1	1.9	1.5	4.7	6.4	48.5
6	8.0	46.7	24.8	22.0	23.0	20.5	19.1	46.5
9	5.3	47.4	6.0	6.9	4.4	4.7	2.8	48.4
12	4.0	46.8	10.6	10.7	13.6	20.5	2.4	47.0
15	3.2	47.0	16.8	16.2	10.3	4.7	8.2	46.6
18	2.7	47.1	7.9	7.1	13.6	20.5	12.6	47.5
21	2.3	47.0	12.7	14.3	7.1	4.7	0.7	46.2
24	2.0	45.0	3.0	2.8	6.2	10.2	0.0	45.0

H_k stands for harmonic number, $T_k = 48$ years$/H_k$ gives the period. $t_{k,max}$ ($t_{k,min}$) indicates the 1st maximum (minimum) of H_k in years (+1900) for the original $V_{A\Sigma}$ (winter NAO index) series. Columns 5–7 reflect the relative variance the harmonics account for when $V_{A\Sigma}$ is modified: [1] $V_{A\Sigma} \doteq 0$ when $\leqslant 3$. This eliminates variations due to weak and moderate ice winters from the record. [2] In addition, values of $V_{A\Sigma}$ for 1970 and 1971 are exchanged to remove the main disturbance of the 8-year cycle. [3] $V_{A\Sigma} \doteq 0$ except for 1947, 55, 63, 71(=70), 79, and 87 when orginal values are retained.

monics in Table 3 poorly represents the NAO data. An additional 28.8% variance is due to H_1 (48 years, 12.6%), H_5 (9.6 years, 10.2%), and H_{11} (4.36 years, 6.1%).

7. Winter severity versus 11-year solar cycle and QBO

7.1. Background

Attempts to show connections between the weather on the earth and solar activity have a long history (Meadows, 1975). Currie (1987) reported signs of 11 years variations for half of 330 worldwide air temperature series. Kelly (1977) drew attention to such variations in the North Atlantic winter air pressure field, while Tinsley (1988) discussed a possible connection between latitudinal variations of Atlantic stormtracks in winter and solar activity. The contraction (expansion and splitting) of the northern polar vortex and the corresponding intensification of zonal (meridional or blocked) tropospheric circulation has been claimed to be affected by enhanced (diminished) corpuscular radiation as indicated by parallel variations of geomagnetic activity in the auroral oval (Bucha, 1988). It has not yet been possible to attribute such statistical correlations to plausible physical mechanisms (Pittock, 1983).

Even though this is a most unsatisfactory situation, it would be difficult to deny that a sufficiently strong and statistically significant association between the solar cycle and climatic variations could be of practical value when predicting such variations.

The work of Meinardus (1906) and Hill and Jones (1990) brought to our attention the possibility of an indirect connection between the solar cycle and ice winter severity in the Western Baltic. The time series of the maximum ice extent off Newfoundland contains dominant quasi-periodic oscillations of 11 years (and 8 years) which strongly resemble the evolution, in time as well as intensity, of the 8 years (and 5.8 years) signals in $V_{A\Sigma}$ (cf. Fig. 5). On the other hand, Meinardus (1906) made the point that severe ice years off Iceland tend to occur simultaneously with both sun-spot minima and maxima. Baur (1949) described a double cycle in European Großwetter with strengthened monsoonal circulation and severe winters occurring in the extremes of the solar cycle. In a modelling study of global surface temperature history by Schneider and Mass (1975), significant excursions such as the downturn in temperature after 1950 were attributed to the parabolic relationship between the solar constant and sunspot activity used in the heating parameterization. If the validity of Kondratyev's and Nikolsky's (1970) relation can be accepted, total irradiance assumes a maximum at intermediate (transient) activity levels and decreases towards both high and low sunspot activity by about 2%. The fact that the spectrum of the $V_{A\Sigma}$ series reveals a significant maximum at 5.8 years led us to check if there is a preference for severe ice winters to occur in the extremes of the solar cycle (Subsection 7.2.).

Van Loon's and Labitzke's work (1988), henceforth vLL, corroborates this possibility. Their Fig. 3 depicts spatial fields of the correlation between 10.7 cm solar flux and Northern Hemisphere sea level pressure for each of two stratifications of the QBO phase (east and west direction of equatorial stratospheric winds) in January/February. From this figure, a distinct negative (positive) correlation of -0.4 ($+0.5$) is evident for winters in central Europe when the QBO was westerly (easterly). In terms of anomalous winds the regional pattern in vLL's Fig. 3a implies that with maximum solar activity and a coinciding westerly phase of the QBO, easterly surface wind components are prevalent in the Western Baltic. The preference for the same wind direction is even greater when the easterly phase of the QBO occurs during a solar minimum (vLL: Fig. 3b). These easterly wind anomalies are linked with negative temperature anomalies (vLL: Figs. 8, 10) which can cause enhanced ice formation.

While the underlying physics of the solar-QBO-atmosphere association remain obscure, it has to be acknowledged that solar-induced changes in stratospheric ozone concentrations, temperatures, and winds appear to be well established (Lean, 1991). There are a variety of ways in which stratospheric dynamics can influence global climate (Brasseur et al., 1993), and GCM results of Boville (1993) and observational results of Kodera (1993) make it seem likely that the stratospheric state has a significant impact on that of the troposphere. Despite the absence of a physical understanding, the solar-QBO-atmosphere association is sufficiently strong to *justify immediate use for operational forecasting purposes* at the Climate Analysis Center (Barnston and Livezey, 1989).

7.2. $V_{A\Sigma}$ versus solar cycle (1879–1996)

We first turn to the question of the association between ice winter severity and the phase of the solar cycle. The association between ice winter severity and the phase of the QBO, only known since 1951, is considered later (Subsection 7.3). Fig. 9 shows the cyclic variations of the 10.7 cm solar flux since 1879 (regressed from sunspot numbers before 1947) as provided by B. T. Hill (personal communic., 1992). These variations of solar activity, while dominated by a paramount 11 years rhythm, have been shown by Fais and Mosetti (1989) to contain additional periodicities (e.g., 8 and 5.6 years), as may be inferred from quite erratic variations of amplitude and length of the observed cycles.

The severity of ice winters is shown in Fig. 9 by circles and squares which are superposed on the solar flux curve. This figure appears to suggest a tendency towards strong and very strong ice winters (filled circles/squares: $V_{A\Sigma} > 3\,\mathrm{m}/10\,\mathrm{m}$), both in periods of low and high solar activity. The greatest deviations from this general pattern are found in Cycle 17 (1934–1944), but also in Cycle 13 (1890–1902) in which strong or very strong ice

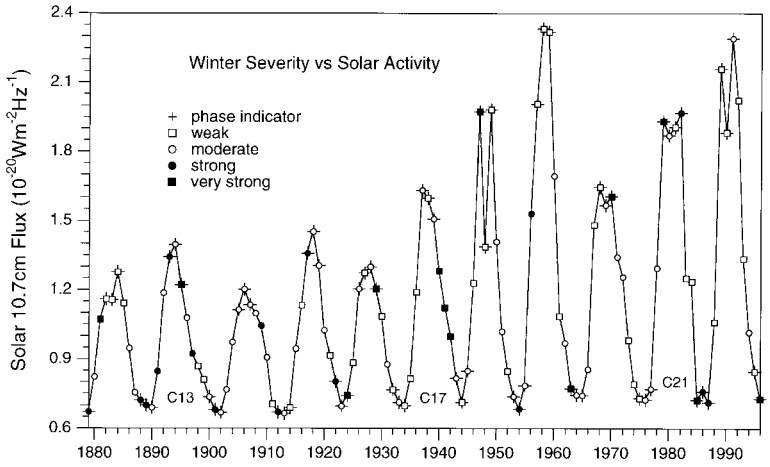

Fig. 9. Ice winter severity versus solar activity. The time series of the average January-February-March solar flux at 10.7 cm was kindly provided by B. T. Hill (personal communic., 1992). Ice winter severity as indicated by circles and squares superposed on the solar flux curve.

winters occurred in the transient phase, too. As seen in KL's Fig. 2, the last decade of the 19th century is characterized by a very high quasi-biennial variability, while the war-time winters represent the most severe ice winters in the whole of the period under investigation. It is clear that the large-scale circulation and the character of an ice winter do not evolve in response to no single cause. Thus, deviations from a hypothetic clear-cut solar flux–sea ice association do not necessarily rule out such relationship but may result from interfering factors of influence.

The solar flux–sea ice association, if real, shows most clearly after WWII, when all but 1 (1956) out of 11 strong or very strong ice winters occurred in phases of high or low solar activity. A suitable means to test this nonlinear association statistically is within a contingency table analysis (Table 4). Since the frequency of extreme ice winters has increased at the expense of moderate and strong winter types after 1920, it appeared reasonable to unify weak and moderate as well as strong and very strong ice winter types.

The division into phases of low, high, and transient solar activity takes greater account of the multi-annual residence time in states of low and high activity than the determination of the activity cycles' absolute extrema. These phase states were discriminated in time by assigning the attributes low/high to the 3 lowest/highest values between two consecutive solar maxima/minima. On account of the strong scattering of observations, this criterion would produce discontinuous high phases for cycles 18, 21, and 22. This awk-

Table 4. *Winter severity versus solar activity 1879–1996**

Ice winter severity	Phase of solar cycle			Row totals
	low	*high*	*transient*	
very strong or strong	13 (8.1)	8 (8.6)	8 (12.3)	29
moderate or weak	20 (24.9)	27 (26.4)	42 (37.7)	89
Col. totals	33	35	50	118

* Cell values give absolute frequencies of concurrent events. Expected cell frequencies are in parenthesis. Error probability due to χ^2 test: 5.1%.

wardness was remedied by redefining the period of high activity as the time in between and including a double peak.

The dependence of the severity of ice winters on the phase of the solar cycle may be accepted with an error probability of 5.1% by applying the χ^2 test to Table 4. As is seen from the theoretical frequency distribution (Table 4, values in parenthesis), the statistical association is based on a reduced occurrence of stronger ice winters in transitional phases and an increased occurrence of such winters during low solar activity. The distribution of ice winter types during high solar activity matches statistical expectations for independence. At least one strong or very strong ice winter occurred in 9 out of 12 solar minima since 1879. The probability for a strong winter during low solar activity thus amounts to 75% as compared to an overall frequency of 25%.

To check the stability of these results, we also tested $V_{A\Sigma}$ versus solar activity contingency tables for the periods (I) 1879–1929 ($p=7\%$), (II) 1920–1960 ($p=79\%$), (III) 1951–1996 ($p=6\%$), and (I+III) ($p=0.4\%$). The effect of sample size on statistical significance is evident from the error probability for period (I+III) as compared to that of (I) or (III), only. Even a Monte Carlo test without restrictions on the marginal frequencies (mc2, cf. Appendix C) gives a p-value as low as 4.9% for (I+III).

The disturbance of the association during the core of period (II) not only fell together with the period of high variance as well as a notably different variance distribution in $V_{A\Sigma}$ (cf. Section 5 & Fig 4–5). It also coincided with a doubling in amplitude of solar activity (Fig. 9) that relates inversely to solar cycle length. Interestingly, the latter parameter closely matches the long-term variations of the Northern Hemisphere land air temperature during the past 130 years including the strong warming during 1920–1950 (Friis-Christensen and Lassen, 1991).

The reader is referred to Appendix C for statistically more convincing evidence and supplementary details to the above findings.

7.3. $V_{A\Sigma}$ – solar cycle – QBO (1951–1996)

Based on the results of van Loon and Labitzke (1988), an increased probability can be expected for the occurrence of stronger ice winters during low solar activity when, at the same time, the phase of the QBO is easterly (*elow*) but also during high solar activity and westerly QBO (*whigh*). Such pooled phase conditions existed in the winters of 1955, *63*, 75, 77, *85* and (*87*, strong only) and 1958, 68, *70*, *79*, 81, 89 and 91 (cf. Figs. 9–10). Although very strong ice winters occurred in only 4 cases (italics), the probability (31%) of such ice winters is greatly increased as compared to their overall relative frequency (5/46=11%).

Table 5 gives the distribution of ice winter types during the different phases of the QBO and the solar cycle. The observed distribution differs from the theoretical no-relation distribution with an error probability of 8.2%. The error probability decreases to 4.5% when strong and moderate ice winter types are considered one class. The correlation is based not only on an enhanced frequency (+183%) of very strong ice winters under *elow* & *whigh* conditions, but also on an increased (reduced) frequency, +34% (−32%), of strong & moderate (very strong & weak) for *wlow* & *ehigh* phase states. Substantiating evidence for this result is provided in Appendix C.

It should perhaps be mentioned that no significant correlation is obtained when distributing the ice winter types according to the phases of the QBO only. This does not necessarily reflect expectations based on Ebdon's (1975) investigation of the influence of the QBO on the atmospheric surface pressure field in the Northern Hemisphere in January between 1955 and 1974. But that study restricts itself to only 5 cases with pronounced westerly and easterly winds at the equatorial 30 hPa level. Although the pressure anomaly fields for both phases of the QBO show a complementary pattern, a clear deviation from the mean pressure field in the North Atlantic is seen only for easterly phases. The reduced strength of both the Azores high and the Icelandic low of around 6 hPa results in a weak zonal circulation in the central North Atlantic and northwest Europe during periods of strong equatorial easterly winds.

8. Conclusions

67% of variance in the $V_{A\Sigma}$ series can be explained by variations in the quasi-biennial Q_3^3 and intermediate I_5^{10} periodicity ranges. Both

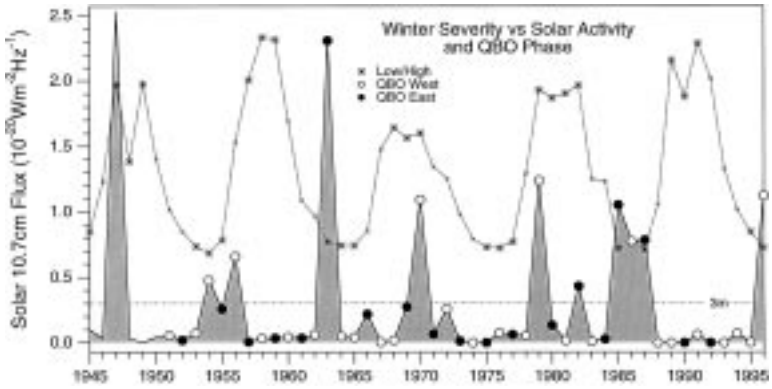

Fig. 10. Ice winter severity versus solar cycle and QBO phase. The dotted curve represents the solar flux at 10.7 cm in winter as provided by B. T. Hill (personal communic., 1992). The left axis also accounts for $V_{A\Sigma}$ in decameters as depicted by the solid line. The thin horizontal line separates ice winters of weak or moderate severity from strong or very strong winters. Blank and filled circles on the ice series show the phase state of the QBO to be west or east, respectively. The phase of the QBO, specified from Fig. 25 in Naujokat et al. (1994) and Labitzke and van Loon (1996), reflects the direction of the zonal component of equatorial winds at 45 mb in January-February.

Table 5. *Winter severity versus QBO and solar activity 1951–1996**

Ice winter severity	Pooled phase conditions			Row totals
	elow & whigh	*wlow & ehigh*	*transient*	
very strong	4 (1.4)	1 (1.5)	0 (2.1)	5
strong	1 (1.4)	3 (1.5)	1 (2.1)	5
moderate	3 (4.8)	6 (5.2)	8 (7.0)	17
weak	5 (5.4)	4 (5.8)	10 (7.8)	19
Col. totals	13	14	19	46

* Cell values give absolute frequencies of concurrent events. Expected cell frequencies are in parenthesis. Error probability due to χ^2 test: 8.2%.

ranges also contribute most to the variance of the NAO index (53%) and account for 68% of the covariance between both series. The *carrier cycles* are almost identical for both time series (2.3 and 7.8 years and 2.4 and 7.7 years, respectively).

Because of the time dependence of variance, the spectral variance distributions for 1879–1992 describe mean conditions, which are representative of shorter time sections but to a limited extent. The composite character of the mean variance distribution of the $V_{A\Sigma}$ series was revealed in the spectral subinterval analysis. The 5.8 years variance maximum is thus based mainly on this cycle's high intensity before 1940, while the even higher variance contribution of the 7.8 years cycle originates exclusively from the subsequent period of time. Since 1960, large variance contributions have been concentrated in the 4 and especially the 3.2 years cycles. Neither of these would be considered significant on grounds of the mean variance distribution.

It was further shown that the $V_{A\Sigma}$ series after WWII can be reproduced by superposition of a fundamental oscillation of period 16 years and its higher harmonics (8, 5.3, 4, 3.2, 2.7, 2.3, 2 years). In the first place, the strength of these cycles (accounting for 84% variance) is a consequence of the nonsinusoidal character of the time series, which in the gross consists in singular amplitude-modulated 8 years signals.

In pointing out parallel cycles in related time series, our intention was to substantiate their significance. It would be naïve, however, to suspect the various cycles to be associated with a comple-

mentary variety of generating processes. The mathematical composition of a time series by sinusoidal oscillations should not be confused with its generation in reality. The immediate physical cause of ice winter variability clearly is variations of the atmospheric circulation of some repetitiveness due to internal nonlinear dynamics of the climate system and (quasicyclic) external forcing. Statistics can relate facts but is an improper means of revealing physical cause-effect chains.

The autoregressive model on which the ME spectral analysis is based could be a starting point in statistical ice winter prediction. Because of the instability of variance and the accompanying variations in intensity of the different quasi-cycles, the prospects of success are limited, however. Model fitting should be limited to the most recent period of time with stationary variance in the gross. The very strong ice winter of 1996 confirms that this period, which has been dominated by the 8 years rhythm for several decades, has continued. But even this is no safeguard against new, sudden changes in the spectral variance distribution which of necessity result in a completely incorrect prediction.

The association between ice winter severity and the phase states of the solar cycle was ascertained statistically for the periods 1879–1929 and 1951–1956, but not for the core time section of the $V_{A\Sigma}$ series. 9 of the 10 strong and very strong ice winters since 1951 occurred in phases of high and low solar activity. It is only in phases of low solar activity, however, that the probability of occurrence of strong and very strong ice winters, viz. $6/14 = 43\%$, clearly exceeds ($+97\%$) the overall relative frequency of $10/46 = 22\%$ of these ice winter types. 4 out of 5 very strong ice winters occurred when the phasing of stratospheric winds along the Equator and solar activity was *east* & *low* or *west* & *high*.

The physical mechanisms through which solar flux and QBO may affect the tropospheric climate are still obscure. Yet, the quasiperiodic character of the solar cycle and the QBO and the strength of their statistical association with ice winter severity can possibly aid in ice winter forecasting in the Western Baltic. An investigation of meteorological differences in years of low solar activity could provide clues for the temporary non-occurrence of stronger ice winters or aid in detecting other climate parameters of predictive potential.

9. Acknowledgements

We sincerely thank Brian Hill (Institute of Marine Dynamics, St. John's) for supplying the dataset on Newfoundland ice extent. Special thanks are extended to Thomas Royer (University of Alaska, Fairbanks) for information on the lunar nodal tide, Günter Schulz (Bundesamt für Seeschiffahrt und Hydrographie, Hamburg & Rostock) and Karin Labitzke (Freie Universität Berlin) for recent data on solar activity and the stratospheric QBO, Gerhard Asmussen (Deutscher Wetterdienst, Hamburg) for providing air temperatures at Schleswig, and Peter Lemke (Institut für Meereskunde, Kiel) for his comments and suggestions on the initial draft. The presentation of this paper has been greatly improved thanks to the comments of the anonymous referees.

10. Appendix A

Winter NAO index 1879–1996

In the course of this study, many data requests have been received as to the winter NAO index series. In order to facilitate its usage in similar research, the winter NAO index is presented in Table 6. Moreover, to afford the reproduction of our findings on the winter North Atlantic Oscillation, Table 6 includes monthly sea level pressure (SLP) data at Ponta Delgada (PD) and Akureyri (A). SLP data sources were detailed in KL. The tabulated winter NAO index can be verified and extended from its definition

$$\mathrm{NAO}_i = \left.\frac{p_i - \bar{p}}{\sigma}\right|_{\mathrm{PD}} - \left.\frac{p_i - \bar{p}}{\sigma}\right|_{\mathrm{A}} \qquad \forall\, i \in [1879, 1996]. \tag{A1}$$

Note that winters are identified by the calendar year (i) associated with the month of January and that December data thus are from the preceding year. p_i is the mean DJF SLP in any one year, $\bar{p}_{\mathrm{PD}}$ ($= 1020.15$ hPa) and $\bar{p}_{\mathrm{A}}$ ($= 1003.38$ hPa) denote the 30-year mean DJF SLPs for 1961–1990, and σ_{PD} ($= 4.00$ hPa) and σ_{A} ($= 6.53$ hPa) are the corresponding interannual standard deviations.

Table 6. *SLP [+900 hPa] at Ponta Delgada and Akureyri and winter NAO index*

	Ponta Delgada			Akureyri			NAO
Winter	DEC	JAN	FEB	DEC	JAN	FEB	DJF
1879	108.4	119.9	123.4	121.5	110.9	102.9	-2.01
1880	114.9	114.5	118.0	100.7	105.7	92.5	-0.51
1881	118.2	101.2	120.1	112.3	124.8	116.3	-3.95
1882	126.5	123.4	121.6	91.9	96.5	102.7	1.89
1883	120.1	119.5	123.6	111.3	94.3	89.4	1.00
1884	123.3	121.5	118.4	99.9	97.9	96.7	1.03
1885	124.3	117.5	111.2	93.3	101.5	108.5	-0.27
1886	117.7	125.1	121.3	105.7	105.3	109.0	-0.20
1887	121.1	121.9	122.4	103.5	88.5	99.8	1.35
1888	113.8	118.9	116.5	108.3	112.5	114.3	-2.21
1889	121.2	127.2	128.3	91.4	100.3	114.2	1.57
1890	128.9	123.8	119.0	93.1	84.5	109.5	2.11
1891	119.7	124.4	119.5	107.3	105.7	99.8	0.13
1892	123.8	124.0	116.7	93.4	102.1	117.0	0.22
1893	118.6	116.1	120.9	107.8	113.7	100.9	-1.03
1894	125.3	121.2	125.9	91.4	97.3	85.3	2.84
1895	123.4	119.2	101.8	100.5	114.3	123.0	-2.75
1896	119.1	120.5	119.4	102.5	109.1	97.3	-0.06
1897	124.2	119.9	123.3	93.7	112.6	99.0	0.83
1898	121.9	122.9	122.6	98.2	92.6	96.2	1.76
1899	119.7	115.2	108.5	94.6	103.7	103.7	-1.01
1900	119.5	126.8	111.1	104.3	94.7	119.5	-0.68
1901	121.2	118.9	113.7	92.7	98.1	120.8	-0.63
1902	124.1	121.5	108.8	103.7	104.9	113.8	-1.13
1903	122.0	118.0	120.7	98.5	95.7	89.3	1.38
1904	123.5	125.3	122.5	101.3	90.5	100.9	1.79
1905	117.8	122.2	129.2	104.1	97.9	103.9	0.95
1906	116.0	123.9	128.8	94.7	89.3	101.0	1.97
1907	129.0	126.8	126.4	102.7	103.1	98.5	2.11
1908	121.8	124.8	132.2	99.0	98.1	102.2	2.08
1909	125.3	124.6	120.2	96.7	93.9	106.1	1.49
1910	112.3	127.8	128.8	103.4	93.4	87.5	2.02
1911	119.0	125.1	121.9	100.3	100.1	100.1	0.95
1912	118.3	117.6	105.3	90.9	107.1	105.3	-1.26
1913	123.6	119.0	119.0	91.1	95.7	102.3	1.17
1914	123.2	117.7	121.0	100.1	99.8	91.8	1.06
1915	121.8	124.6	123.3	93.8	100.6	101.5	1.50
1916	115.8	125.9	127.7	111.0	89.9	95.9	1.43
1917	111.0	117.8	118.1	107.3	115.1	110.1	-2.27
1918	123.1	105.7	128.2	113.7	114.2	93.1	-0.84
1919	125.6	122.6	108.8	99.9	101.4	110.3	-0.36
1920	128.5	128.2	124.3	93.9	89.4	98.2	3.17
1921	115.7	126.1	121.1	105.7	95.0	102.1	0.58
1922	128.7	122.2	124.0	92.9	97.3	86.9	2.89
1923	123.9	128.8	118.3	99.1	97.9	94.7	1.82
1924	127.5	119.5	119.5	101.3	95.0	107.7	0.82
1925	123.6	121.9	128.4	84.3	91.7	97.5	2.99
1926	108.6	119.5	117.8	108.9	96.3	96.7	-0.79
1927	121.2	128.4	120.7	106.6	95.3	103.0	1.09
1928	112.9	129.9	124.0	114.5	87.1	94.7	1.24
1929	124.8	110.6	117.8	101.8	122.0	104.5	-1.53
1930	123.4	122.4	121.4	84.9	89.9	108.5	1.93
1931	126.6	123.8	129.5	93.9	105.5	99.7	2.18
1932	122.8	122.0	113.3	103.4	92.3	126.0	-0.79
1933	118.3	121.0	116.3	94.6	85.7	117.1	0.25
1934	123.2	125.8	125.5	109.0	92.5	106.5	1.28
1935	115.5	124.7	126.4	99.0	106.6	92.9	1.11
1936	119.1	111.1	111.1	108.7	111.0	114.2	-2.81
1937	123.9	117.0	117.1	94.1	88.6	98.7	1.26
1938	121.0	127.0	117.8	108.5	90.3	108.1	0.61
1939	121.8	115.8	125.0	96.2	110.5	90.6	0.83
1940	118.0	114.5	111.5	107.9	113.8	111.8	-2.56
1941	123.1	115.3	117.0	104.7	118.6	107.9	-1.50
1942	124.2	128.0	113.7	99.9	98.9	119.3	0.05
1943	119.3	116.5	131.7	95.7	102.3	96.8	1.37
1944	125.3	122.6	124.1	99.8	93.9	111.5	1.21
1945	125.6	121.2	126.4	99.3	119.0	90.6	1.13
1946	114.6	124.1	122.5	105.5	93.7	108.0	0.21
1947	126.1	117.6	110.4	98.3	98.0	128.0	-1.25
1948	118.1	120.2	117.3	110.3	94.9	104.4	-0.38
1949	118.5	124.6	122.5	99.8	96.2	89.8	1.67
1950	122.1	119.8	123.7	98.8	101.5	96.3	1.12
1951	123.2	125.0	125.0	110.4	99.0	99.0	1.15
1952	124.0	131.0	117.0	88.0	98.0	109.0	1.74
1953	123.0	116.0	124.0	109.0	103.0	104.0	-0.09
1954	121.0	126.0	126.0	94.0	106.0	100.0	1.56
1955	125.0	114.0	114.0	94.0	107.0	115.0	-0.92
1956	120.0	120.0	115.0	104.0	105.0	116.0	-1.21
1957	125.0	125.0	117.0	95.0	90.0	107.0	1.47
1958	126.0	118.0	112.0	98.0	100.0	112.0	-0.36
1959	120.0	115.0	125.0	106.0	118.0	98.0	-0.64
1960	125.0	116.0	107.0	93.0	112.0	114.0	-1.49
1961	128.0	125.0	120.0	96.0	101.0	96.0	1.92
1962	109.0	126.0	128.0	114.0	91.0	108.0	0.07
1963	118.0	108.0	118.0	106.0	127.0	113.0	-3.20
1964	116.0	115.0	113.0	112.0	106.0	108.0	-2.18
1965	122.0	120.0	112.0	102.0	102.0	126.0	-1.55
1966	124.0	108.0	109.0	102.0	114.0	112.0	-2.53
1967	126.0	119.0	122.0	95.0	113.0	94.0	0.96
1968	122.0	125.0	114.0	109.0	104.0	110.0	-0.61
1969	120.0	110.0	109.0	110.0	113.0	117.0	-3.31
1970	128.0	106.0	128.0	103.0	103.0	107.0	-0.02
1971	121.0	115.8	122.7	111.0	103.5	98.0	-0.20
1972	123.1	120.8	121.5	98.6	97.5	101.7	1.04
1973	122.1	121.7	131.1	90.7	98.6	98.3	2.35
1974	124.6	121.0	123.9	105.4	81.6	99.7	1.95
1975	125.3	123.4	115.8	94.0	93.0	104.4	1.29
1976	121.2	124.8	120.9	103.0	101.0	94.2	1.15
1977	116.9	118.6	116.8	113.3	112.6	109.4	-1.96
1978	114.7	128.4	106.7	102.2	99.9	114.0	-1.19
1979	111.7	114.0	114.1	110.9	113.1	105.6	-2.71
1980	122.5	117.8	122.1	93.6	112.2	104.1	0.17
1981	127.4	129.8	123.4	100.5	105.3	98.8	1.96
1982	118.3	117.7	120.2	110.6	109.3	90.9	-0.39
1983	128.1	127.6	119.5	94.5	86.1	113.3	2.06
1984	120.8	133.6	125.3	99.9	90.2	96.4	2.81
1985	123.8	114.7	113.6	94.7	117.6	110.4	-1.34
1986	120.2	132.2	116.2	111.8	98.3	124.8	-0.58
1987	124.3	109.8	117.3	93.6	114.4	107.7	-1.04
1988	112.6	124.8	123.9	106.5	100.1	106.5	-0.08
1989	122.2	127.4	128.8	98.9	88.8	87.5	3.28
1990	108.1	126.8	122.3	105.2	83.2	79.1	1.91
1991	123.6	123.7	124.6	93.7	96.7	106.4	1.64
1992	121.3	117.5	125.6	101.5	103.0	92.2	1.02
1993	123.7	123.9	125.2	95.1	86.0	106.7	2.17
1994	129.9	129.6	117.9	96.1	99.2	106.7	1.83
1995	122.8	127.5	125.2	92.0	92.9	92.1	2.95
1996	111.8	112.4	126.3	115.4	104.5	104.5	-1.56

11. Appendix B

Amplitude modulation and beats

The superposition of two harmonic oscillations is formally written as

$$\psi = A_1 \cos z_1 + A_2 \cos z_2 , \tag{B1}$$

where $z_k = 2\pi\nu_k(t-t_k)$. In the context of harmonic or Fourier analysis, the frequency $\nu_k = H_k/P$, H_k being the kth harmonic (a pure number), and P the fundamental period, the length of the observational record in time.

Introducing the notation $\bar{x} \doteq (x_1+x_2)/2$ and $x^* \doteq (x_1-x_2)/2$, eq. (B1) takes the form

$$\psi = (\bar{A}+A^*)\cos(\bar{z}+z^*) + (\bar{A}-A^*)\cos(\bar{z}-z^*), \tag{B2}$$

which by observing the identity

$$\cos(\bar{z}-z^*) \pm \cos(\bar{z}+z^*) = 2 \begin{matrix} \cos z^* \cos \bar{z} \\ \sin z^* \sin \bar{z} \end{matrix}, \tag{B3}$$

is expressible as

$$\begin{aligned} \psi &= 2\bar{A}\cos z^* \cos\bar{z} - 2A^* \sin z^* \sin\bar{z} \\ &= \bar{A}_{\mathrm{mod}} \cos\bar{z} - A^*_{\mathrm{mod}} \sin\bar{z} . \end{aligned} \tag{B4}$$

Here, $\bar{z} = 2\pi\bar{\nu}(t-\bar{t}) - 2\pi\nu^* t^*$ and $z^* = 2\pi\nu^*(t-\bar{t}) - 2\pi\bar{\nu}t^*$, which for $t_1 = t_2 \equiv t_0$ reduces to $\bar{z} = 2\pi\bar{\nu}(t-t_0)$ and $z^* = 2\pi\nu^*(t-t_0)$. Eq. (B4) thus represents the superposition of two oscillations at a mean (high) frequency $\bar{\nu}$, the amplitudes of which vary in time at a (low) modulation frequency ν^*.

Eq. (B4) can be contracted to give

$$\psi = A_{\mathrm{mod}} \cos(\bar{z}-\phi), \tag{B5}$$

where $\phi = -\arctan(A^*_{\mathrm{mod}}/\bar{A}_{\mathrm{mod}})$ and $A^2_{\mathrm{mod}} = \bar{A}^2_{\mathrm{mod}} + A^{*2}_{\mathrm{mod}}$. On using the identity $2\cos^2 x = 1+\cos 2x$, the last expression gives

$$\begin{aligned} A^2_{\mathrm{mod}} &= 2\bar{A}^2(1+\cos 2z^*) + 2A^{*2}(1-\cos 2z^*) \\ &= A_1^2 + A_2^2 + 2A_1A_2 \cos 2z^* . \end{aligned} \tag{B6}$$

Now, for $A_1 \approx A_2$, it follows that $\bar{A} \gg A^*$, $\phi \approx 0$ in eq. (B5), and

$$\begin{aligned} A^2_{\mathrm{mod}} \approx \bar{A}^2_{\mathrm{mod}} &= 4\bar{A}^2 \cos^2 z^* \\ &= 2\bar{A}^2(1+\cos 2z^*) . \end{aligned} \tag{B7}$$

A^2_{mod} thus swings at twice the modulation frequency $\nu_{\mathrm{beat}} = 2\nu^*$ about its mean value.

12. Appendix C

Winter air temperature at Schleswig versus QBO and solar cycle

It is a well-known fact that ice conditions strongly depend on local surface air temperatures. For $V_{A\Sigma}$ and the winter temperature at Schleswig (54°31′N, 9°33′E, cf. KL Fig. 1) the linear correlation during 1951–1996 was −0.81. The following results thus seem well suited to substantiate the statistical findings of Section 7.

Table 7A shows winter air temperatures (T_s) at Schleswig (personal communication G. Asmussen, Deutscher Wetterdienst, 1996) and corresponding phases of the QBO and the solar cycle (SC) for the period 1951–1996. For comparison, the table includes $V_{A\Sigma}$ and the winter NAO index. The January-February (JF) mean temperatures were normalized (norm) and classified (class) setting class limits at ± 0.2533 and ± 0.8415 standard deviations such that each class would hold 20% of all data. The meaning of the classes is *very cold* (C), *cold* (c), *normal* (N), *warm* (w) and *very warm* (W). The columns are sorted by normalized JF temperatures in ascending order.

The effect of this re-arrangement on the solar phase data shows in the emergence of several clusters. Very cold temperatures (*C*) are most frequently associated with low solar activity (70%), while cold (*c*) and negative normal temperatures (N^-) most often occur with high solar activity (70%). In contrast, warm temperatures (*w*) exclusively fall in the transient sections of the solar cycle. The distribution of QBO west phases over *C-c-N-w-W* as 5-0-8-0-2 shows that the west phase preferably associates with normal winter temperatures, when solar activity is extreme (low or high). The east phase, on the other hand, tends toward *C&c* (4-3-2-0-3).

The number of permutations or different arrangements of n (=46) distinct solar phases is $n!$. To decide if a sequence of m_s (=8) transient descending (*td*) phases within the arrangement at hand (Table 7A) is a statistically significant feature, we calculate the number N of m_s-sequences realized within the $n!$ permutations of the n-set of phases. Treating $m_s \leqslant m$ (=14) *td* phases as a 1-element subset, and accounting for the permutations of m_s phases selected from the m-set of *td* phases, yields $N = (n-m_s+1)!\ m!/(m-m_s)!$, and $\bar{N} = N/n!$ for the average count of m_s-sequences per permutation of the n-set.

Table 7. *Winter Air Temperatures at Schleswig versus QBO and Solar Cycle 1951–1996*

A

Year	Jan	Feb	JF	norm	class	QBO	SC	VAΣ		NAO	
1963	-5.4	-4.8	-5.10	-2.42	C	e	lo	23.07	S	-3.20	w
1979	-4.3	-3.3	-3.80	-1.85	C	w	hi	12.36	S	-2.71	w
1985	-4.6	-2.9	-3.75	-1.83	C	e	lo	10.52	S	-1.34	w
1956	0.6	7.0	-3.20	-1.59	C	w	ta	6.56	s	-1.21	w
1996	-2.2	-3.0	-2.60	-1.32	C	w	lo	11.24	S	-1.56	w
1970	-2.9	-2.2	-2.55	-1.30	C	w	hi	10.93	S	-0.02	n-
1986	-0.6	-4.5	-2.55	-1.30	C	w	lo	7.75	s	-0.58	n-
1987	-3.9	-0.3	-2.10	-1.11	C	e	lo	7.82	s	-1.04	w
1954	-0.2	-3.6	-1.90	-1.02	C	w	lo	4.74	s	1.56	s
1955	-1.2	-2.1	-1.65	-0.91	C	e	lo	2.59	m	-0.92	n-
1982	-2.5	0.1	-1.20	-0.71	c	e	hi	4.30	s	-0.39	n-
1980	-2.5	0.3	-1.10	-0.67	c	e	hi	1.33	m	0.17	n+
1972	-2.5	0.7	-0.90	-0.58	c	w	td	2.58	m	1.04	s
1966	-1.4	0.6	-0.40	-0.36	c	e	ta	2.17	m	-2.53	w
1969	0.9	-1.7	-0.40	-0.36	c	e	hi	2.73	m	-3.31	w
1968	-0.5	0.2	-0.15	-0.25	N	w	hi	0.20	w	-0.61	n-
1959	0.1	0.2	0.15	-0.12	N	e	hi	0.36	w	-0.64	n-
1978	1.3	-1.0	0.15	-0.12	N	w	ta	0.53	m	-1.19	w
1981	-0.5	0.9	0.20	-0.10	N	w	hi	0.19	w	1.96	s
1958	0.2	0.5	0.35	-0.03	N	w	hi	0.31	w	-0.36	n-
1960	0.8	0.1	0.45	0.01	N	w	td	0.44	m	-1.49	w
1964	0.3	0.8	0.55	0.05	N	w	lo	0.46	m	-2.18	w
1953	1.1	0.1	0.60	0.08	N	w	lo	0.73	m	-0.09	n-
1991	2.5	-1.0	0.75	0.14	N	w	hi	0.62	m	1.64	s
1976	0.9	0.7	0.80	0.16	N	w	lo	0.75	m	1.15	s
1977	0.3	1.6	0.95	0.23	N	e	lo	0.64	m	-1.96	w
1965	1.8	0.2	1.00	0.25	N	w	lo	0.41	m	-1.55	w
1984	1.6	0.4	1.00	0.25	N	e	td	0.30	w	2.81	s
1994	3.2	-1.2	1.00	0.25	N	w	td	0.71	m	1.83	s
1952	1.1	1.6	1.35	0.41	w	e	td	0.20	w	1.74	s
1951	1.3	1.6	1.45	0.45	w	w	td	0.54	m	1.15	s
1971	0.3	2.6	1.45	0.45	w	e	td	0.67	m	-0.20	n-
1993	2.3	1.0	1.65	0.54	w	w	td	0.00	w	2.17	s
1962	2.4	1.4	1.90	0.65	w	w	td	0.63	m	0.07	n+
1961	-0.1	4.0	1.95	0.67	w	e	td	0.36	w	1.92	s
1967	1.1	3.1	2.10	0.73	w	w	ta	0.04	w	0.96	n+
1973	2.0	2.4	2.20	0.78	w	e	td	0.14	w	2.35	s
1983	4.8	-0.1	2.35	0.84	W	w	td	0.10	w	2.06	s
1995	0.7	4.1	2.40	0.86	W	w	lo	0.03	w	2.95	s
1957	2.2	3.4	2.80	1.04	W	e	hi	0.06	w	1.47	s
1992	2.8	4.0	3.40	1.30	W	e	td	0.00	w	1.02	s
1975	5.4	1.5	3.45	1.32	W	e	lo	0.02	w	1.29	s
1988	4.1	2.8	3.45	1.32	W	w	ta	0.00	w	-0.08	n-
1974	3.6	3.7	3.65	1.41	W	w	td	0.01	w	1.95	s
1989	4.2	4.3	4.25	1.67	W	w	hi	0.00	w	3.28	s
1990	4.2	6.1	5.15	2.07	W	e	hi	0.00	w	1.91	s

JF: January-February mean temperatures at Schleswig (Ts)
norm: Ts(JF) normalized for 1951-1996 (mean=0.4250°C, stddev=2.2839°C)
class: C (very cold), c(cold), N (normal), w (warm), W (very warm)
class limits at +/-0.2533 & +/- 0.8415 stddev

B

Ts	wlo	elo	whi	ehi	ta	td	Σ r
C	3 1.7	4 1.3	2 1.5	0 1.3	1 1.1	0 3.0	10
c	0 0.9	0 0.7	0 0.8	3 0.7	1 0.5	1 1.5	5
N	4 2.4	1 1.8	4 2.1	1 1.8	1 1.5	3 4.3	14
w	0 1.4	0 1.0	0 1.2	0 1.0	1 0.9	7 2.4	8
W	1 1.6	1 1.2	1 1.4	2 1.2	1 1.0	3 2.7	9
Σ c	8	6	7	6	5	14	46
°C	-0.2	-1.4	-0.1	0.9	0.4	1.6	0.4

p(χ2;mc1;mc2)=(0.4;0.2;8.3)%

C

Ts	low	high	ta&td	Σ r
C	7 3.0	2 2.8	1 4.1	10
c	0 1.5	3 1.4	2 2.1	5
N	5 4.3	5 4.0	4 5.8	14
w	0 2.4	0 2.3	8 3.3	8
W	2 2.7	3 2.5	4 3.7	9
Σ c	14	13	19	46
°C	-0.71	0.34	1.32	0.43

p(χ2;mc1;mc2)=(0.3;0.1;5.0)%

D

Ts	elo&whi	wlo&ehi	ta&td	Σ r
C	6 2.8	3 3.0	1 4.1	10
c	0 1.4	3 1.5	2 2.1	5
N	5 4.0	5 4.3	4 5.8	14
w	0 2.3	0 2.4	8 3.3	8
W	2 2.5	3 2.7	4 3.7	9
Σ c	13	14	19	46
°C	-0.70	0.26	1.32	0.43

p(χ2;mc1;mc2)=(0.6;0.5;9.2)%

E

VAΣ	wlo	elo	whi	ehi	ta	td	Σ r
vs	1 0.9	2 0.7	2 0.8	0 0.7	0 0.5	0 1.5	5
s	2 0.9	1 0.7	0 0.8	1 0.7	1 0.5	0 1.5	5
m	4 3.0	2 2.2	1 2.6	2 2.2	2 1.8	6 5.2	17
w	1 3.3	1 2.5	4 2.9	3 2.5	2 2.1	8 5.8	19
Σ c	8	6	7	6	5	14	46

p(χ2;mc1)=(29;30)%

F

NAO	wlo	elo	whi	ehi	ta	td	Σ r
w	3 2.3	4 1.7	1 2.0	1 1.7	3 1.4	1 4.0	13
n-	2 1.7	1 1.3	3 1.5	2 1.3	1 1.1	1 3.0	10
n+	0 0.5	0 0.4	0 0.5	1 0.4	1 0.3	1 0.9	3
s	3 3.5	1 2.6	3 3.0	2 2.6	0 2.2	11 6.1	20
Σ c	8	6	7	6	5	14	46

p(χ2;mc1)=(9.6;8.7)%

°C: mean JF temperature
QBO: w (west), e (east)
SC: lo (low), hi (high), ta/td (transient a-/descending)
VAΣ: S (very strong), s (strong), m (moderate), w (weak)
NAO: w (weak), n (normal), s (strong westerlies)

Note that $\bar{N}$ is related to the probability $\Pr(m_s)$ of selecting 1 m_s-sequence from the n-set (drawing m_s times without laying back) through $\bar{N} = (n-m_s+1)\Pr(m_s)$. Thus $\bar{N}$ is the average count of m_s-sequences in $l_x = n-m_s+1$ such experiments. The probability of selecting at least 1 m_s-sequence in l_x experiments, however, is $\Pr(l_x, m_s) = 1-(1-\Pr(m_s))^{l_x}$. (By analogy, the average count of 6es per 6 throws of a dice is $\bar{N} = 1$, but the probability for at least one 6 in 6 throws is $1-(5/6)^6 = 0.67$.)

For the sequence of 8 *td* phases (that almost coincides with the *w*-class) we find $\bar{N}(8td) \approx \Pr(39, 8td) = 0.04 \times 10^{-2}$. For 11 transient phases in a row out of 19 *ta&td* $\bar{N}(11t) \approx \Pr(36, 11t) = 0.02 \times 10^{-2}$. On the other hand, the seemingly curious clustering of QBO west phases (that fall in the normal temperature

range) would occur in about every 3rd permutation ($\bar{N}(8w)=0.33$, $\Pr(39,8w)=0.28$). But its occurrence at this particular location is quite unlikely ($\Pr(8w)=\bar{N}/39=0.85\times10^{-2}$).

In the cold regime (*C&c*), 80% of the temperatures are associated with extreme solar phases, as compared to 29% in the warm regime (*W&w*). The mean JF temperature (−0.20°C) in extreme solar phases is significantly cooler than that in transient phases (*ta&td*, 1.32°C; $p(t\text{-test})=2.5\%$). Of all possible QBO/extreme solar phase combinations the mean temperatures for *elo&wlo* (=low solar activity, −0.71°C, $p=0.8\%$), *elo&whi* (−0.70°C, $p=1.5\%$), and *elo* (−1.37°C, $p=1\%$) are most significantly different from the mean temperature in transient phases. However, significant differences between low and high activity temperatures (−0.71°C, 0.34°C, $p=28\%$) or between *elo&whi* and *ehi&wlo* temperatures (−0.70°C, 0.26°C, $p=32\%$) cannot currently be detected.

The occurrence of different winter types (in terms of T_s) statistically depends on the state of the solar cycle (SC) and the QBO (Table 7B–D). The null hypothesis that the row and column factors of the contingency tables are independent of each other is rejected by the χ^2 test and 2 Monte-Carlo tests (mc1 & mc2) performed for the population of tables that have the same marginal frequencies as the observed table (mc1) and for the (larger) population of tables that have but the same total frequency as the observed table (mc2). The mc tests do not require the expected cell frequencies (small printed) to be large values (Romesburg and Marshall, 1985).

The observed departures from the theoretical frequency distribution are most pronounced for the events *lo/C*, *hi/c&N*$^-$, *elo&whi/C* and *td/w* (133%=(7–3)/3, 148%, 112%, 188%, respectively). This implies that chances for a *C* winter rise from 22%(=3/14=10/46) to 50%(=7/14) in a low phase of the solar cycle, and to 46% for *elo&whi* combinations. The probability for *c&N*$^-$ type winters increases from 22% to 54% if the solar cycle is in high mode, while chances for *C&c* type winters fall from 35% to 7% in transient descending mode.

The dependence of different winter types (in terms of $V_{A\Sigma}$) on the state of the solar cycle and the QBO cannot be detected within Table 7E. The length of the ice season is less than 11 days (or 4.9 ± 3.5 days on average) for winters outside the *C&c* regime. Not only are such short ice seasons prone to observational inaccuracies, they also are a poor measure to characterize a full winter season or to dicriminate one winter season from the other in a climatological sense. As a consequence, the distribution of weak and moderate winters within the *N&w* temperature section is quite at random. Still, the main conclusions as to the joint T_s-SC-QBO distribution may also be drawn in case of $V_{A\Sigma}$ but as yet with less statistical confidence (cf. Section 7). Would the apparent association stand up another 46 years — as may be simulated by doubling the cell frequencies of the $V_{A\Sigma}$ table (Table 7E) — error probabilities would decrease to $p(\chi^2;\text{mc1};\text{mc2})=(0.3\%;\ 0.2\%;\ 5.8\%)$.

The contingency table for the winter NAO index is significant at the 90% level (Table 7F). The 95% level of significance is exceeded after unification of $n-$ and $n+$. The joint distribution *w-n-s* versus *elo&whi-wlo&ehi-ta-td* is significant at the 95% level due to pronounced deviations in the *td* class only. For the joint distribution *w-n-s* versus *lo-hi-ta-td* $p(\chi^2;\text{mc1};\text{mc2})=(1\%;\ 0.8\%;\ 10.6\%)$. Chances for weak westerlies increase by 77% (from 28%(=13/46) to 50%(=7/14)) when solar activity is low, but decrease by 61% (drop to 11%) for *hi* or *td* modes of solar activity. The probability of normal but below average westerlies ($n-$) also increases by 77% (from 22% to 38%) when solar activity is high. The probability for strong westerlies increases by 81% (from 43% to 79%) when the phase of the solar cycle is transient descending. These results are compatible with those obtained for T_s and $V_{A\Sigma}$.

REFERENCES

Angell, J. K., Korshover, J. and Cotten, G. F. 1969. Quasi-biennial variations in the "Centers of Action". *Mon. Wea. Rev.* **97**, 867–872.

Alenius, P. and Makkonen, L. 1981. Variability of the annual maximum ice extent of the Baltic Sea. *Arch. Meteor. Geophys. Bioklim.* **29**, 393–398.

Andersen, N. 1974. On the calculation of filter coefficients for maximum entropy spectral analysis. *Geophys.* **39**, 69–72.

Barnston, A. G. and Livezey, R. E. 1989. A closer look at the effect of the 11-year solar cycle and the Quasi-Biennial Oscillation on Northern Hemisphere 700 mb

height and extratropical North American surface temperature. *J. Clim.* **2**, 1295–1313.

Baur, F. 1949. Zurückführung des Großwetters auf solare Erscheinungen. *Arch. Met. Geophys. Bioklim.* **A1**, 358–374.

Blackman, R. B. and Tukey, J. W. 1958. *The measurement of power spectra.* Dover Publications, 190 pp.

Boville, B. A. 1993. The stratosphere in general circulation models. In: *The rôle of the stratosphere in global change* (ed. M.-L. Chanin). NATO ASI Series **I** 8. Springer-Verlag Berlin Heidelberg, 199–214.

Brasseur, G. P., Smith, A. K. and Granier, C. F. 1993. The Stratosphere: An Introduction. In: *The rôle of the stratosphere in global change* (ed. M.-L. Chanin). NATO ASI Series **I** 8. Springer-Verlag Berlin Heidelberg, 1–27.

Brier, G. W. 1968. Long-range prediction of the zonal westerlies and some problems in data analysis. *Rev. Geophys.* **6**, 525–551.

Bucha, V. 1988. Influence of solar activity on atmospheric circulation types. *Ann. Geophysicae* **6**, 513–524.

Currie, R. G. 1987. Examples and implications of 18.6- and 11-year terms in World Weather Records. In: *Climate, history, periodicity and predictability* (eds. M. R. Rampino, J. E. Sanders, W. S. Newman and L. K. Konigsson). Van Nostrand Reinhold Company, New York, 378–403.

Dyer, R. M. 1970. Persistence in snowfall intensities measured at the ground. *J. Appl. Meteorol.* **9**, 29–34.

Ebdon, R. A. 1975. The Quasi-Biennial Oscillation and its association with tropospheric circulation patterns. *Meteorol. Mag.* **104**, 282–297.

Fais, S. and Mosetti, F. 1989. On periodicities in the sunspot series. *Boll. Geof. Teor. Appl.* **XXXI**, 315–320.

Folland, C. K. 1983. Regional-scale interannual variability of climate— a north-west European perspective. *Meteorol. Mag.* **112**, 163–183.

Friis-Christensen, E. and Lassen, K. 1991. Length of the solar cycle: an indicator of solar activity closely associated with climate. *Science* **254**, 698–700.

Geller, M. A. 1989. Variations without forcing. *Nature* **342**, 15–16.

Ghil, M. and Vautard, R. 1991. Interdecadal oscillations and the warming trend in global temperature time series. *Nature* **350**, 324–327.

Hay, R. F. M. 1967. The association between autumn and winter circulations near Britain. *Meteorol. Mag.* **96**, 167–178.

Hill, B. T. and Jones, S. J. 1990. The Newfoundland ice extent and the solar cycle from 1860 to 1988. *J. Geophys. Res.* **95**, 5385–5394.

Jones, R. H. 1976. Autoregression order selection. *Geophys.* **41**, 771–773.

Kelly, P. M. 1977. Solar influence on North Atlantic mean sea level pressure. *Nature* **269**, 320–322.

Kodera, K. 1993. Influence of the stratospheric circulation change on the troposphere in the northern hemisphere winter. In: *The rôle of the stratosphere in global change* (ed. M.-L. Chanin). NATO ASI Series **I** 8. Springer-Verlag Berlin Heidelberg, 227–243.

Kondratyev, K. Ya. and Nikolsky, G. A. 1970. Solar radiation and solar activity. *Quart. J. R. Met. Soc.* **96**, 509–522.

Koslowski, G. and Loewe, P. 1994. The Western Baltic sea ice season in terms of a mass-related severity index: 1879–1992. Part I: Temporal variability and association with the North Atlantic Oscillation. *Tellus* **46A**, 66–74.

Künzel, F. 1989. Maximum entropy spectral estimation: Some new statistical and numerical details. *Beitr. Phys. Atmosph.* **62**, 227–235.

Labitzke, K. and van Loon, H. 1996. On the stratosphere, the QBO, and the sun: The winter of 1995–1996. *Meteorol. Z.*, N. F. 5, 166–169.

Landsberg, H. E. 1962. Biennial pulses in the atmosphere. *Beitr. Phys. Atmosph.* **35**, 184–194.

Landsberg, H. E., Mitchell, J. M., Crutcher, H. L. and Quinlan, F. T. 1963. Surface signs of the biennial atmospheric pulse. *Mon. Wea. Rev.* **91**, 549–556.

Lean, J. 1991. Variations in the sun's radiative output. *Rev. Geophys.* **29**, 505–535.

Leppäranta, M. and Seinä, A. 1985. Data of freezing, maximum annual ice thickness and break up of ice along the Finnish coast 1830–1984. Internal Report 1985 (2), Finnish Institute of Marine Research.

Lisitzin, E. 1974. *Sea level changes.* Elsevier Scientific Publishing Company, Amsterdam, 246 pp.

Loutre, M. F., Berger, A., Bretagnon, P. and Blanc, P.-L. 1992. Astronomical frequencies for climate research at the decadal to century time scale. *Clim. Dyn.* **7**, 181–194.

Maksimov, I. V. and Smirnov, N. P. 1965. A contribution to the study of the causes of long-period variations in the activity of the Gulf Stream. *Oceanology* **5**, 15–24.

Maksimov, I. V. and Smirnov, N. P. 1967. A long-term circumpolar tide and its significance for the circulation of the ocean and the atmosphere. *Oceanology* **7**, 173–178.

Marko, J. R., Fissel and Birch, J. R. 1986. *Physical approaches to iceberg severity prediction.* ESRF Report Nr. 38, 104 pp.

Meadows, A. J. 1975. A hundred years of controversy over sunspots and weather. *Nature* **256**, 95–97.

Meinardus, W. 1906. Periodische Schwankungen der Eistrift bei Island. *Ann. Hydrogr. Marit. Meteorol.* **34**, 148–162.

Mitchell, J. M., Dzerdzeevskii, B., Flohn, H., Hofmeyr, W. L., Lamb, H. H., Rao, K. N. and Wallén, C. C. 1966. *Climatic change.* WMO, Tech. Note No. 79, Geneva, 79 pp.

Mysak, L. A., Manak, D. K. and Marsden, R. F. 1990. Sea-ice anomalies observed in the Greenland and Labrador Seas during 1901–1984 and their relation to an interdecadal Arctic climate cycle. *Clim. Dyn.* **5**, 111–133.

Naujokat, B., Labitzke, K., Lenschow, R., Rajewski, B., Wiesner, M. and Wohlfahrt, R.-C. 1994. The strato-

spheric winter 1993/94. A winter with some minor warmings and an early final warming. *Beilage zur Berliner Wetterkarte 4. 8. 1994*. Amtsblatt des Instituts für Meteorologie der Freien Universität Berlin, 24 pp.

Newell, N. E., Newell, R. E., Hsiung, J. and Zhongxiang, W. 1989. Global marine temperature variation and the solar magnetic cycle. *Geophys. Res. Lett*. **16**, 311–314.

Panofsky, H. A. and Brier, G. W. 1968. *Some applications of statistics to meteorology*. The Pennsylvania State University, University Park, Pennsylvania, 224 pp.

Papoulis, A. 1962. *The Fourier integral and its applications*. McGraw-Hill, New York, p. 44.

Pittock, A. B. 1983. Solar variability, weather and climate: an update. *Quart. J. R. Met. Soc*. **109**, 23–55.

Polli, S. 1946. La realta' fisica del ciclo climatico di 5.6 anni. *Geofisica Pura e Applicata* **8**, 94–103.

Polli, S. 1950. Il ciclo climatico di 8 anni e sua realta' fisica. *Annali di Geofisica* **3**, 63–76.

Press, W. H., Flannery, B. P., Teukolsky, S. A. and Vetterling W. T. 1988. *Numerical recipes in C*. Cambridge University Press, Cambridge, 735 pp.

Rogers, J. C. 1982. Combined signals of the Walker Oscillations to Northern Hemisphere sea level pressure and air temperature. 259–264. In: *Proc. 7th Ann. Climate diagnostics Workshop*, Boulder, CO, USA. US Dept. of Commerce, Washington DC 20230, USA.

Rogers, J. C. 1984. The association between the North Atlantic Oscillation and the Southern Oscillation in the Northern Hemisphere. *Mon. Wea. Rev*. **112**, 1999–2015.

Rogers, J. C., and van Loon, H. 1979. The seesaw in winter temperatures between Greenland and Northern Europe. Part II: Some oceanic and atmospheric effects in middle and high latitudes. *Mon. Wea. Rev*. **107**, 509–519.

Romesburg, H. C. and Marshall, K. 1985. CHITEST: A Monte-Carlo computer program for contingency table tests. *Computers & Geosciences* **11**, 69–78.

Royer, T. C. 1993. High latitude oceanic variability associated with the 18.6 year nodal tide. *J. Geophys. Res*. **98**, 4639–4644.

Schneider, S. H. and Mass, C. 1975. Volcanic dust, sunspots, and temperature trends. *Science* **190**, 741–746.

Schuurmans, C. J. E. 1978. Influence of solar activity on winter temperatures: New climatological evidence. *Climatic Change* **1**, 231–237.

Stellmacher, R. and Tiesel, R. 1989. Über die Strenge der mitteleuropäischen Winter der letzten 220 Jahre — eine statistische Untersuchung. *Z. Meteorol*. **39**, 56–59.

Stidd, C. K. 1953. Cube-root-normal precipitation distributions. *Trans. AGU* **34**, 31–35.

Tinsley, B. A. 1988. The solar cycle and the QBO influences on the latitude of storm tracks in the North Atlantic. *Geophys. Res. Lett*. **15**, 409–412.

Van den Bos, A. 1971. Alternative interpretation of maximum entropy spectral analysis. *IEEE Trans. Inform. Theory* **IT-17**, 493–494.

Van Loon, H. and Labitzke, K. 1988. Association between the 11-year solar cycle, the QBO, and the atmosphere. Part II: Surface and 700 mb in the Northern Hemisphere in winter. *J. Clim*. **1**, 905–920.

Van Loon, H. and Rogers, J. C. 1978. The seesaw in winter temperatures between Greenland and Northern Europe. Part I: General Description. *Mon. Wea. Rev*. **106**, 296–310.